Master Thesis in Geographical Information Science nr 117

Evaluation of water stress mapping methods in vineyards using airborne thermal imaging

Alon Zuta

2020
Department of
Physical Geography and Ecosystem Science
Centre for Geographical Information Systems
Lund University
Sölvegatan 12
S-223 62 Lund
Sweden

Alon Zuta (2020). Evaluation of water stress mapping methods in vineyards using airborne thermal imaging. Master's degree thesis, 30/ credits in Master in Geographical Information Sciences Department of Physical Geography and Ecosystems Science, Lund University

Evaluation of water stress mapping methods in vineyards using airborne thermal imaging

Alon Zuta
Master Thesis, 30 credits, in Geographical Information Sciences

Supervisor 1: Prof. Dr. Martin Berggren
Lund University

Supervisor 2: Enass Said Al-Kharusi
Lund University

Alon Zuta

Abstract

Due to its low cost and high efficiency, the use of airborne infrared thermography imaging from an unmanned aerial vehicle (UAV) has become a widely used technique for measuring plant water stress. With that, the use of UAV as a precision agriculture technique to map crop water stress is not trivial and the current research project aimed to identify the performance characterises of UAV for vineyard water stress mapping by highlighting the following three objectives:

a. Comparing two commonly used thermal indices, the crop water stress index (CWSI) and the Jones stomatal conductance index (Ig) in order to assess their performances in regions with high climatic variability.

b. Assessing the impact of spatial and temporal changes on the performance of interpolation algorithms.

c. Exploring a possibility of mapping the water stress of a vineyard by collecting and analysing thermal data of the vineyard's cover crop rather than the grapevines themselves.

This study was conducted in two commercial vineyards in the Rheingau region of Germany. Airborne thermal imaging using UAV was collected at four different periods during the 2019 growing season (July-September) and was accompanied by ground measurements including mid-day stem water potential (Ψstem) and proximal thermal imaging. The airborne data was interpolated using the following interpolation algorithms: Inverse Distance Weighting (IDW), Kriging, Local Polynomial, and Spline. Different interpolation surfaces were created using either CWSI or Ig and either cover crop or grapevine's pixels with the total of 64 maps for each vineyard (4 dates x 2 crop types x 2 indices x 4 algorithms). The resulting interpolated surfaces were evaluated through cross validation and, as well, through comparison to the ground measurements.

The cross-validation results showed definite preference for CWSI based interpolations which can be attributed to the range of potential values rather than the suitability of the index while the comparison to the ground measurement results show definite preference for Ig based interpolations. Both the cross validation and the comparison to the ground measurement results show a miscellany of interpolation algorithms which varies both

spatially (between the two vineyards) and temporarily (between the different measurement dates). The cross-validation analyses and the comparison with the proximal thermal imaging measurements show a preference for cover crop-based interpolation while the comparison with the Ψ_{stem} shows a preference for cover crop during the July measurements and grapevine during the August-September measurements. This can be related to the small sample size of the Ψstem procedure and, potentially, an operator bias.

The results of this study indicated that the Ig index exhibits much higher suitability than CWSI for mapping water stress index in regions with higher humidity and variable climate such as the Rheingau. Additionally, the study illustrated the affect of sampled data points on the resulting interpolated surface and the importance of evaluating different algorithms and choosing the most suitable one. Finally, it demonstrated that cover crop-based data has the potential of producing better quality water stress maps in steep-slopped vineyards which characterized by low soil depth, but an additional research has to be conducted in order to evaluate suitability for other types of environments.

Keywords: Cover crop, Thermal imaging, Spatial variability, vineyards, interpolation, water stress index, CWSI, Ig, stem water potential, UAV, Rheingau.
Advisors: **Martin Berggren and Enass Said Al-Kharusi.**
Master degree project 30 credits in Geographical Information Sciences, 2020
Evaluation of water stress mapping methods in vineyards using airborne thermal imaging. Department of Physical Geography and Ecosystem Science, Lund University
Thesis nr 117

Acknowledgements

The current research would not have been possible without the help of many people. Firstly, Prof. Dr. Manfred Stoll from the Geisenheim University who served as an external supervisor. Thank you for providing me with the opportunity to work on this subject, for all your helpful comments and guidance and for allowing me to use the university's resources. Many thanks also to Dipl.-Physicist. Marco Hofmann from the Geisenheim University who instructed me and assisted me in conducting the field work. I would also like to thank my supervisors at Lund University, Prof. Dr. Martin Berggren and Mrs. Enass Said Al-Kharusi for guiding me through this project and for their help in the development of this thesis. Finally, I would also like to take this opportunity to thank my wife for her patience, support and love.

Table of Contents

Abbreviations

Bu	Burgweg vineyard
CWSI	Crop water stress index
DN	Digital number
Ef	Ehrenfels vineyard
g_s	Stomatal conductance
Ig	Jones stomatal conductance index
IDW	Inverse distance weighted
ME	Mean error
NDVI	Normalized difference vegetation index
NIR	Near infrared
R^2	Coefficient of determination
RMSE	Root mean square error
T_{dry}	Maximum dry baseline
T_{leaf}	Leaf temperature
T_{wet}	Maximum wet baseline
UAV	Unmanned aerial vehicle
Ψ	Water potential
Ψ_{stem}	Mid-day stem water potential

List of Figures

List of Tables

1. Introduction

The vineyard water budget is a key factor in quality grape development and insufficient water supply can limit the quality and yield of grapes for wine (Hofmann and Schultz, 2015). Within the grapevine growing zones, water shortage is the most dominant environmental constraint (Williams and Matthews, 1990), and is becoming more prevalent due to climate change which causes shifts in the precipitation rate and distribution (Hannah et al., 2013; Simonneau et al., 2017).

This situation can be mitigated by the implementation of precision irrigation systems, although spatial variability in water requirements within a vineyard can limit the efficient use of precision agricultural systems (Bellvert et al., 2014). Therefore, it is vital to characterize spatial variability before implementing an irrigation strategy. Measurement of the plant water potential is one of the most used methods to monitor plant water stress status (Chone et al., 2001) and there are a variety of techniques to measure water potential (Jones, 2004). Unfortunately, traditional sampling techniques are highly time consuming, labour demanding and, at times, destructive to the plants (Diago et al., 2017; Gutiérrez et al., 2018). A more efficient, less costly, and non-destructive technique is to analyse water stress status using infrared thermography imaging that provides indication of canopy temperature that can be used to calculate the leaf stomatal conductance (Stoll and Jones, 2007). Infrared thermography enables the visualization of differences in canopy surface temperature from the emitted infrared radiation. Recent technological advances in unmanned aerial vehicles (UAV) platforms and their relatively low cost (Hruska et al., 2012) enable airborne thermal data collection that has the advantage of covering larger areas in much shorter time periods, as compared to ground imaging techniques by feet or vehicle mounted.

The research study reported here sought to explore three crucial components of mapping water status based on airborne thermal imaging: *a.* the quality, quantity and distribution of the sampling points, *b*. the type of thermal index used and *c*. the choice of interpolation method.

1.1 Sampling points distribution, grapevine canopy versus cover crop

Quality, quantity and distribution of data points available for collection by UAV is limited by the structure of the grapevine canopy, which is stratified, irregularly shaped and

narrow in width (Figure 1). This research project examined the possibility of mapping water status based on the vineyard cover crop which displays no stratification, has low irregularity and has much wider surface than the grapevines themselves.

The aerial view displays conditions that represent only the upper part of the canopy, while the grapevine conditions directly below the canopy can be significantly different from the top. Grapevine canopies display a large array of possible structures of shape and components (Hofmann et al., 2014) that can result in much variation in radiation received by the plants, stomatal conductance and ambient temperature within a grapevine canopy (Bardero 2019; Ben Gal et al., 2009; Fuentes et al., 2012). Moreover, grapevine row width is relatively narrow resulting in low number of pixels captured (Bellvert et al., 2015; Gutiérrez et al., 2018). In many cases, there are large gaps within the canopy which result in capture of pixels of the background soil and consequence in inaccurate interpretation of data values (Bardero et al., 2019; Bellvert et al., 2015).

The use of cover crops is a common practice in viticulture and is widely used in many of the world's winegrowing regions (Carlos, 2016). Cover crops reduce erosion, add nitrogen, prevent water runoff and improve soil health by enhancing soil organic matter and microbiological functions (Novara et al., 2013; Ruiz-Colmenero et al., 2012; Steenwerth and Belina, 2006). A negative impact of cover crops is that they compete with the vines over nutrients and water (Lopes et al., 2004; Lopes, 2016; Monteiro and Lopes, 2006) specifically in steep sloped vineyards where the soil depth is shallow (Hofmann et al., 2014; Gruber and Schultz, 2005) and the vine roots do not penetrate much deeper than the cover crop roots. Thus, cover crops can be a potential indicator of water potential in vineyards in addition to the vines themselves.

The simple structure, absence of stratification and larger spatial extant of the cover crop relative to grapevines enable easier acquisition of data using airborne thermal imaging. An advantage of measuring cover crop water stress is the potential of producing a better display of the spatial water distribution within a vineyard (Figure 1).

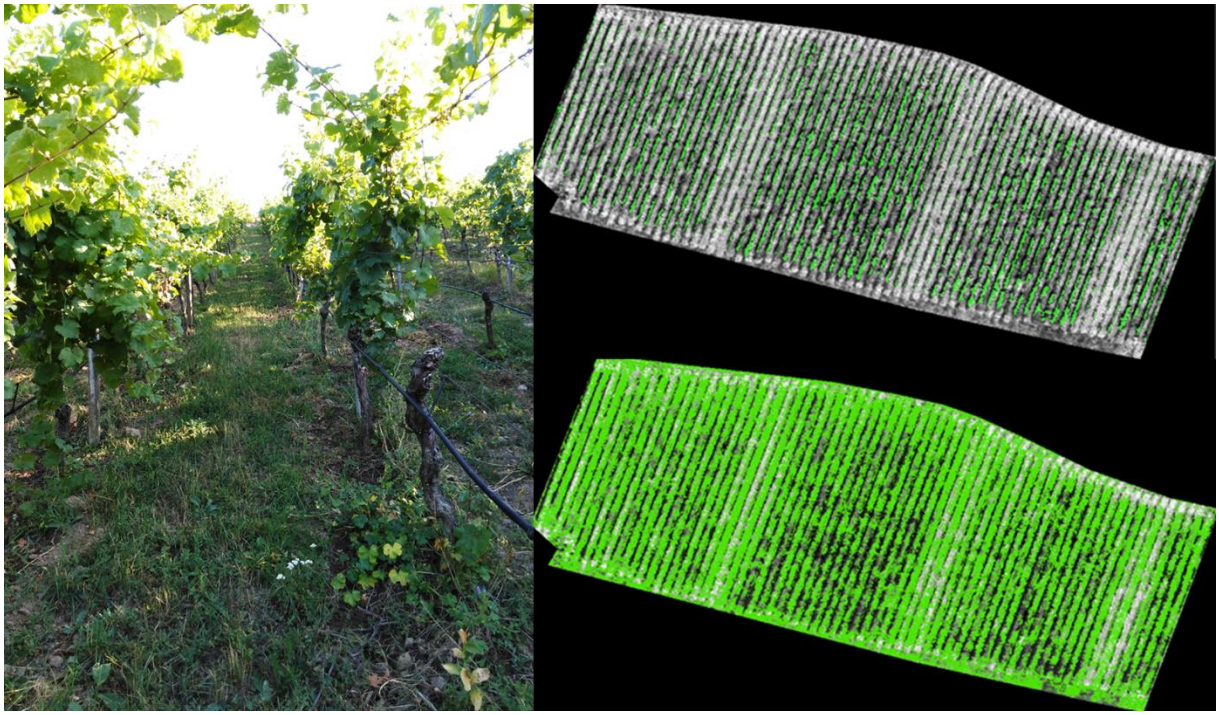

Figure 1. Grapevine canopy and cover crop comparison. The left image shows a typical view of a row in the experiment site showing both the grapevine canopy and the cover crop. The canopy exhibits stratification which enables aerial data collection only of the top layer of the canopy. Additionally, it displays a large array of possible structures of shape and components which results in many variations in radiation conditions, complex stomatal conductance patterns and microclimate. In addition, the canopy is relatively narrow and has many gaps. The cover crop has a simple structure, no stratification and larger spatial extant relative to the grapevines. Top right image shows the pixels collected by the UAV for the grapevine canopy and the bottom right shows the pixels collected by the UAV for the cover crop. The number of captured pixels of the cover crop is much larger compared to the captured pixels of the grapevine canopy.

1.2 Choice of thermal index

Thermal indices enable quantification of crop water stress based on canopy surface temperature. The most used index is the crop water stress index (CWSI) which is highly successful in arid climates but has limited success in humid and variable climates (Jones et al., 1997; Bockhold et al., 2011). The stomatal conductance index (Ig) was developed as a more suitable index for temperate climates (Jones et al, 1997; Jones 1999a). Studies on the use of airborne thermal imaging for mapping water stress in vineyards have been limited to regions which are characterized as semi-arid or Mediterranean climates where droughts are prevalent (Table 1) and therefore used only the CWSI or reported better results using it over the Ig. However, in recent years, as a result of climatic changes,

climate regions classified as cool such as the Rheingau in Germany, have begun to experience phenomena such as warmer temperatures and shifts in precipitation patterns which forces growers to irrigate their crops more frequently (Fraga et al., 2016;, Hofmann and Schultz, 2015) resulting in the need of water stress mapping. The current research project aimed to compare the two indices' suitability in this type of climate.

1.3 Choice of interpolation method

Due to the structural nature of the grapevine canopy which is characterized by a narrow row width and multiple gaps (Bardero et al., 2019; Gutiérrez et al., 2018), interpolation is essential in order to estimate the values in canopy zones which were not sampled. Selecting a proper spatial interpolation method is highly important since different methods can lead to very different results (Aguilar et al., 2005; Li & Heap, 2011) as it can be seen in Figure 2. Many factors affect the performance of spatial interpolation methods and include sampling density, sample spatial distribution, sample clustering, surface type, data variance, data normality, grid size or resolution and the interactions between these factors (Aguilar et al., 2005; Li & Heap, 2008; Li & Heap, 2011; Robinson, 2006). Previous studies focusing on mapping water status in vineyards using UAV have failed to outline the reasons for choosing a specific interpolation method (Baluja et al., 2012; Bellvert et al., 2014; Santesteban et al., 2017) and in some cases fail to mention which method was used (Bellvert et al., 2013; Matese et al., 2018). In order to evaluate the performances of the different spatial interpolation methods, it is necessary to use the statistics of the differences, absolute and squared, between measured and predicted values at sampled points (Curtarelli et al., 2015; Li & Heap, 2008; Li & Heap, 2011). Many studies (presented in table 1) compare the interpolated surfaces to the ground measurements and fail to statistically evaluate their performances (further discussed in section 3.4). Additionally, there is a tendency among past studies to apply the same interpolation method to all collected data regardless of temporal or spatial changes.

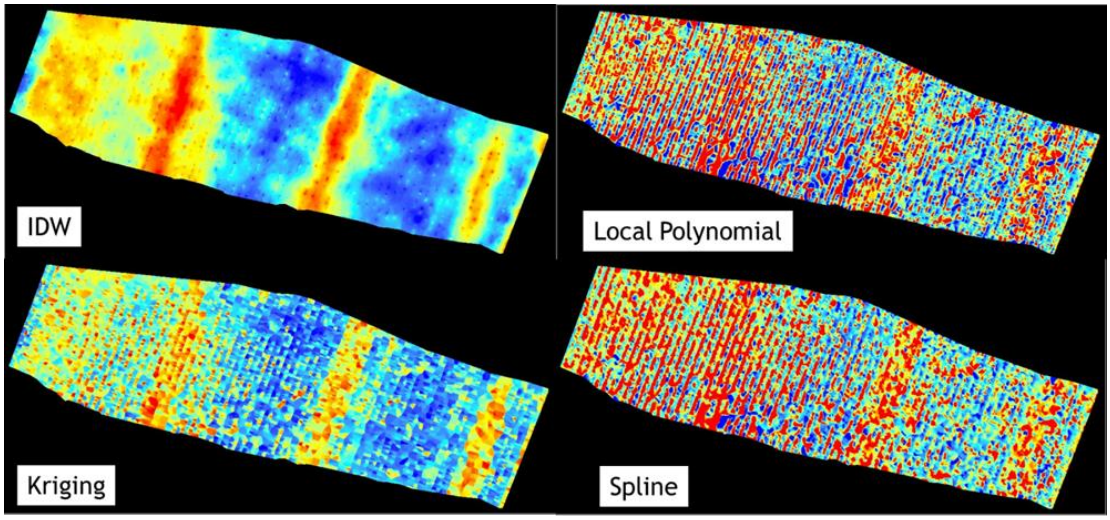

Figure 2. Interpolation surfaces comparison. The four images present the consequence of different interpolation methods created for the same collected data points, demonstrating how different surfaces can result from the selected interpretation algorithm.

2. Research objectives

This research study aims to explore three crucial components of mapping water status based on airborne thermal imaging: a. the quality, quantity and distribution of the sampling points, b. the type of thermal index used and c. the choice of interpolation method. The first objective was to explore whether or not airborne thermal imaging of the vineyard cover crop can be used to evaluate the water status in a vineyard and whether or not it has an advantage over using thermal imaging of the grapevine canopy itself. The second objective was to compare two different thermal indices, the crop water stress index (CWSI) and the Jones stomatal conductance index (Ig) in order to evaluate whether Ig provides better results for water stress mapping of grapevines in temperate and humid climates. The third objective was to demonstrate the impacts spatial and temporal changes have over the performance of interpolation process through the examination and comparison of different interpolation methods over different locations and dates.

3. Literature overview

In the context of changing climate, many sectors of agriculture, such as viticulture can experience impacts to the crop. According to Jones et al., (2005) the importance of understanding climatic change impacts on agriculture is especially evident in viticulture. As grapes are extremely climate sensitive crop, the climate of each wine regions determines the types of grapes that can be grown and the style of wine that can be produced which results in the distinctive character of different wines (Jones et al., 2005; Schultz and Jones, 2010). Future climate change models predict a warming of 2 to 4 C^o in wine growing regions over the next 50 years (Jones et al., 2005; Schultz and Lebon, 2005). Higher temperatures cause higher rates of evaporation, both from soil and from plants which combined with the projected shifts in the participation rate and distribution (Hannah et al., 2013; Simonneau et al., 2017) have the potential of causing droughts. The resulting impacts of changing climatic conditions can be harmful for both yield and quality of the fruit crop (Schultz and Lebon, 2005; Williams and Matthews, 1990) making irrigation inevitable in many cases.

Further complicating the changing incidents of climate factors such as rain, wind, solar radiation and temperature is that water status over a vineyard is highly heterogenous due to variability in soil characteristics, soil depth, slope, vegetation density and evapotranspiration rate (Hofmann and Schultz, 2015). Thus, it is vital to characterize spatial variability before implementing an irrigation strategy to achieve an optimum water supply for productivity.

3.1 Physiological parameters for monitoring plant water stress

Methods to quantitatively measure water content in the soil directly or through calculating the water balance are inefficient for determining water stress as plants respond directly to changes in water status in their tissues rather than to changes in the soil water content. Therefore, plant physiology depends both on the soil moisture status and on the rate of water flow through the plant and the corresponding hydraulic flow resistances between the bulk soil and the appropriate plant tissues (McCutchan and Shackel, 1992; Jones, 2004). A plant-based measurement is the most straightforward indicator of plant water stress as it measures the integrated effect of soil, plant, and atmospheric conditions on water availability within the plant itself (McCutchan and Shackel, 1992).

There have been many efforts by past researchers to develop methods to assess plant response to water deficit in contrast to directly measuring soil moisture (Blanco-Cipollone et al., 2017; Jones 1990; Turner, 1990). Currently, vineyard irrigation scheduling decisions are based on plant responses rather than on direct measurements of soil water status (Jones, 2004). Among the various physiological measurement techniques, water potential (Ψ) based methods performed by pressure chambers are generally used for measuring water stress and are the most reported in literature (Chone et al., 2001; Williams et al., 2011). However, water potential measurements are highly time consuming, labour demanding and can be destructive to the plants (Diago et al., 2017; Gutiérrez et al., 2018) leading researchers to look for more efficient ways to determine water stress.

3.2 Thermal imaging as a tool for monitoring plant water stress

Thermography was first applied for plant examination in the early 1960s (Gates, 1964; Monteith and Szeicz, 1962; Tanner, 1963) and due to advancement in technology and the affordable cost, it has become a major instrument in plant health research. This approach provides indication of canopy temperature that can be used to calculate the leaf stomatal conductance (Stoll and Jones, 2007). Use of canopy temperatures to detect water stress in plants is based upon the assumption that, as water becomes limiting, transpiration is reduced through stomatal closure and thus, plant temperature increases (Jackson et al., 1988). Therefore, canopy temperature can be correlated negatively with stomatal conductance (g_s) and water potential (Ψ) (Costa et al., 2012; Fuentes et al., 2012; Gutiérrez et al.,2018; Grant et al., 2006). Stomatal closure is the first reaction to drought stress among plants and, therefore, is more closely related to soil moisture content than leaf water status (Jones, 1999; Grant et al., 2006; Pirasteh-Anosheh et al., 2016).

3.3 Development of temperature-based water stress indicators

Several studies (Idso et al., 1981; Idso, 1982; Jackson, 1982; Meron et al., 2009) have shown that measurement with thermal imaging of the canopy temperature can be a good indicator of the crop water stress. The most common used thermal index for evaluating crop water stress is the Crop Water Stress Index (CWSI), which expresses the ratio between the difference of the upper, non-transpiring crop and the lower transpiring crop section at potential rate, crop temperature limits (Idso 1982). Since its introduction by

Idso et al, 1981, CWSI has been used as the basis for irrigation scheduling for several crops including grapevine (Jones et al, 1997) and is now one of the most used indices for quantifying the stress a plant undergoes according to the surface temperature of the crop canopy (Poblete-Echeverría et al., 2017). Unfortunately, although the method works very well in arid climates, in areas where humidity is high and wind speed and solar radiation vary, it has limited success (Jones et al, 1997; Bockhold et al, 2011). The stomatal conductance index (Ig) proposed by Jones (Jones et al, 1997; Jones 1999a) which is proportional to the stomatal conductance (g_s) was developed to overcome these limitations.

3.4 Airborne thermal imaging for mapping plant water stress

Use of airborne imaging has the advantage of covering larger areas in much shorter time periods as compared to ground imaging techniques by feet or vehicle mounted. Airborne imaging is also not limited by rough terrain and is becoming cheaper and more approachable with the advances in UAV technology (Hruska et al, 2012). Combined with the use of temperature-based water stress indicators, airborne thermal imaging has proven to have great potential for monitoring plant water stress. Many experiments involving aerial thermal imaging showed good correlation between the derived indices values, stomatal conductance (g_s) and plant water potential (Ψ) (Baluja et al., 2012; Bellvert et al., 2013; Bellvert et al., 2015; Matese et al., 2018; Pou et al., 2013).

Table 1 summarizes several studies examining airborne thermal imaging for mapping water stress in vineyards. All the studies were conducted in regions which are characterized as semi-arid and Mediterranean climates where droughts are prevalent. For that reason, only one study (Baluja et al., 2012) examines the stomatal conductance index (Ig) in addition to the CWSI index. Thus, there is a gap of knowledge regarding water stress mapping of vineyards in temperate climate regions and evaluation and comparison to determine the more suitable index.

Table. 1. Summary of studies examining airborne thermal imaging for mapping water stress in vineyards. The table presents for each study the type of crop investigated, the location where the experiment took place, the indices used (estimated variables), the ground measurement technique compared with the airborne data (reference variables) and the interpolated method used. Not applicable (NA) means that interpolation was not part of the experiment.

Paper	Crop	Location	Estimated variables	Reference variables	Interpolation method
Baluja et al., 2012	Tempranillo	Logroño, Spain	CWSI, Ig	leaf stomatal conductance and stem water potential	Spline
Bellvert et al., 2013	Pinot-noir	Lleida, Spain	CWSI	leaf water potential	Not mentioned
Bellvert et al., 2014	Pinot-noir, Chardonnay, Syrah and Tempranillo	Lleida, Spain	CWSI	leaf water potential	NA
Bellvert et al., 2015	Chardonnay	Lleida, Spain	CWSI	leaf water potential	kriging
Matese et al., 2018	Vermentino, Cabernet' and Cagnulari	Sardinia, Italy	CWSI	Stem water potential and CWSI derived from ground thermal imaging	Not mentioned
Poblete-Echeverría et al., 2016	Carménère	Maule, Chile	Tc-Ta	Stem water potential	NA
Poblete et al., 2018	Cabernet Sauvignon	Maule, Chile	CWSI	NA	NA
Santesteban et al, 2017	Tempranillo	Traibuenas, Navarra, Spain	CWSI	stem water potential and stomatal conductance	Kriging
Zarco-Tejada et al., 2013	Thompson Seedless	Parlier, CA, USA	CWSI	leaf stomatal conductance and leaf water potential	NA

4. Data and methodology

4.1 Study area

The Rheingau region (Figure 3) is a narrow strip bounded between the Rhine river to the South and the Taunus Mountains to the North. The climate in the Rheingau is classified as a temperate oceanic climate (Köppen: Cfb) (Kottek et al., 2006). It lies in the rain shadow of the Taunus Mountains and their forested slopes prevent the flow of cold air into the vineyards below. In this region, the Rhine River flows to the west resulting in most of vineyards to be situated on south facing slopes which are exposed to strong sunlight.

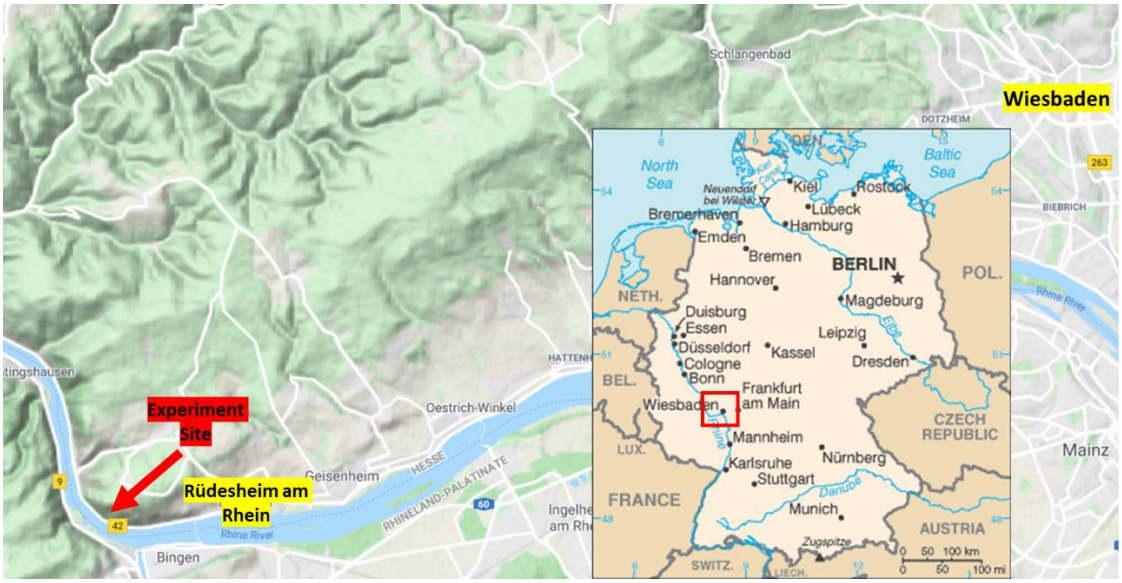

Figure 3. The study area. The location of the Rheingau region within Germany is marked with a red box). The Rheingau region is a narrow strip bounded between the Rhine river to the South and the Taunus Mountains to the North. In this region the Rhine River flows to the west resulting in most of vineyards to be situated on south facing slopes. The experiment sites are located west to the town of Rüdesheim am Rhein on the northern bank of the Rhein river. Source: a. CIA Factbook, map of Germany, retrieved: October 28, 2019, https://www.cia.gov/library/publications/the-world-factbook/geos/gm.html b. Google terrain map , retrieved: January 29, 2020, https://www.google.com/maps/@50.0366132,8.023858,11.75z/data=!5m1!1e4

The study was conducted in two commercial vineyards operated by the Hessian State Winery near Rüdesheim am Rhein, Germany (49°59′0″N 07°55′50″E). The investigated plots named Burgweg (Bu) and Ehrenfels (Ef) (Figure 4) were planted with Riesling (Vitis Vinifera) and trained to a cane or spur pruned VSP Trellis system (Hofmann et al., 2014) and situated at elevation ranging from 100-200 meters above sea level. Steep slope

vineyards are characteristic elements of Central European cool climate viticulture and the management system practiced in the investigated sites is typical for many of the steep slope wine regions. The investigated sites are characterized by shallow (<1.5 m depth) and stony, poor in loess loam, soils that have poor water holding capacity which is typical for steeped slope vineyards (Gruber and Schultz, 2005; Hofmann et al., 2014). The two sites differ in vegetation density and coverage (Table 2). Both vineyards are partly covered by a natural population of cover crops (*Festuca rubra subsp. rubra* and *Medicago lupulina*) and weeds (*Chenopodium album, Cirsium arvense, Malva neglecta* and *Taraxacum officinale*) (Lopes et al., 2004). In Ehrenfels the soil of each row is covered by cover crops whereas in Burgweg alternating rows were kept free of vegetation by frequent tillage. Inter-row vegetation was kept short through frequent mowing. These types of cover crop management are representative for many German steep slope wine regions (Hofmann et al., 2014).

Table. 2. **Main characteristics of the investigated vineyards (Source: Hofmann et al., 2014).** For each vineyard, the table presents the planting density, grapevine canopy height and width, distance between grapevines rows and the fraction of soil covered by cover crop.

Site	Planting density (vines/ha)	Canopy height (m)	Canopy width (m)	Row distance (m)	Fraction of soil covered by vegetation (%)
Burgweg	6875	1.10	0.40	1.60	0.40
Ehrenfels	4400	1.00	0.40	2.50	0.84

To induce a wider range of water status in the vineyard, two different irrigation regimes were applied, irrigated and non-irrigated. The irrigation management was carried out by the Hessian State Winery and applied through dripline system from April until October. The non-irrigated regime, where no irrigation was applied at all other than occasional rain, consisted of three sectors of 4 rows each in different locations within each of the vineyards (Figure 5).

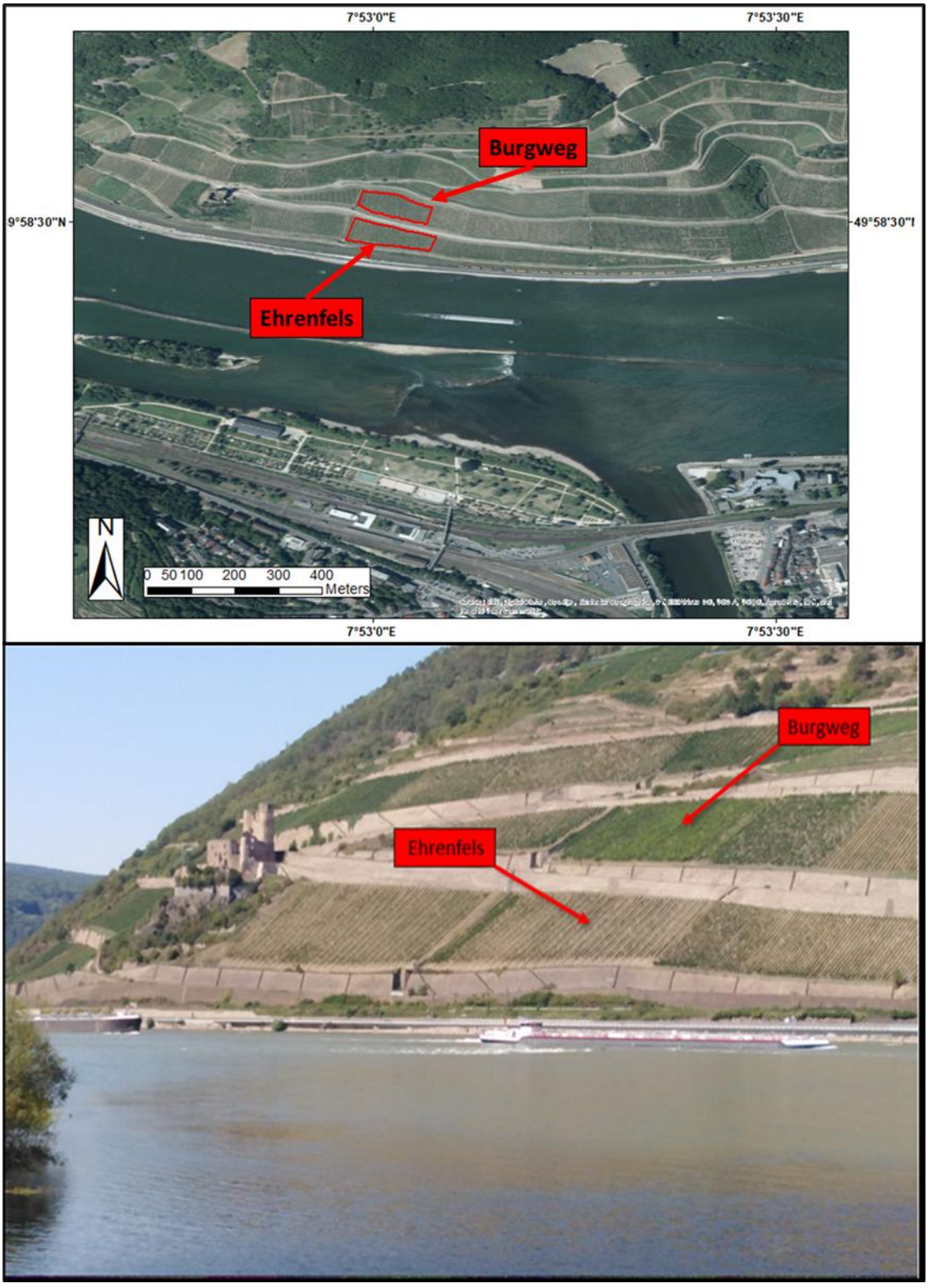

Figure 4. The experiment sites. The images show the locations of the two commercial vineyards: Burgweg and Ehrenfels. The top part shows an aerial view of the experimental site (source: Google Earth). The bottom shows a panoramic view (facing north) of the experimental site (photo: Alon Zuta).

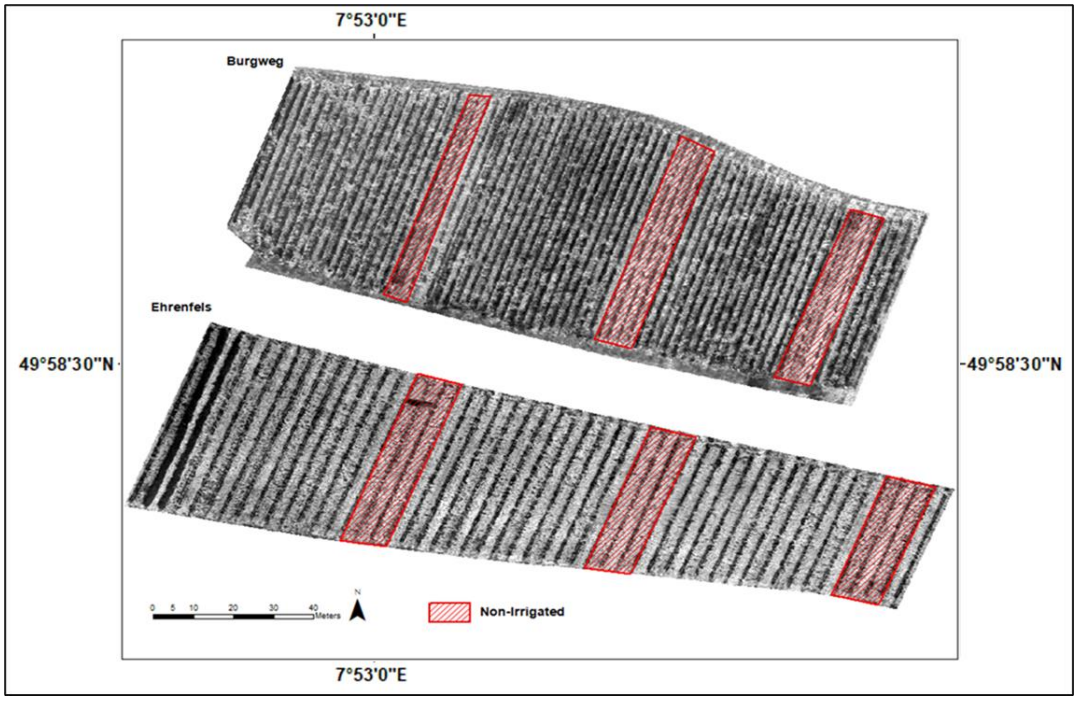

Figure 5. The irrigation Scheme. In order to induce a wider range of water status in the vineyards, two different irrigation regimes were applied, irrigated and non-irrigated. Within each of the vineyards, 3 sectors of 4 rows were completely non irrigated (marked red). The rest of the rows were irrigated using dripline.

4.2 Airborne thermal data acquisition

The UAV platform (Figure 6) used was a modified multi-rotor operated by the unmanned technologies division of Fin Gadar GmbH, Germany. It was equipped with two NEO-M8N u-blox concurrent GNSS modules (ublox Switzerland), a Reach M+ RTK module (Emlid Ltd, Hong Kong) and a Raspberry Pi3 computer (Raspberry Pi Foundation, UK). Flight parameters communication to the ground operator were provided by a radio link at 2.4 GH.z and another channel at 2.4 GH.z for remote sensing data transmission. The flight controller was based on a Pixhawk 2.4.6 with Arducopter 3.4.6 system backup controller Seriously Pro with INAV 1.6.1 software. The airborne data was acquired with a VUE PRO R 640 thermal camera (FLIR Systems, Wilsonville, OR, USA) and a RedEdge-M multispectral camera (MicaSense Inc, Seattle, WA, USA) mounted on a drone. Tables 3 and 4 show technical specifications of the cameras. Four flight campaigns were conducted during the 2019 veraison period (July-September) at the following dates: July 22, July 25, August 22 and September 19 at solar noon. Data

temperature were calculated from the thermal camera digital number (DN) using the empirical line method, as reported by Berni et al., (2009). The DN-values in the thermal imagery represent at-sensor radiance values. Radiometric calibration was done using three different colored panels (1 m × 1 m) at known temperatures as a reference.

Figure 6. The UAV system. A modified multi-rotor operated by the unmanned technologies division of Fin Gadar GmbH, Germany. It is equipped with two NEO-M8N u-blox concurrent GNSS modules, a Reach M+ RTK module and a Raspberry Pi3 computer Photo source: Unmanned-Technologies, 2019.

Table 3. Technical specifications of UAV thermal sensor.

VUE PRO R 640	
Thermal imager	Uncooled VOx Microbolometer
Sensor resolution	640 × 512
Lens field of view	19 mm; 32° × 26°
Spectral frame	7.5 - 13.5 µm
Full frame rates	30 Hz (NTSC); 25 Hz (PAL)
Exportable frame rates	7.5 Hz (NTSC); 8.3 Hz (PAL)
Measurement accuracy	5% of reading

Table 4. Technical specifications of UAV multispectral sensor.

RedEdge-M	
Spectral bands and wavelength	blue (475 nm center, 20 nm bandwidth)
	green (560 nm center, 20 nm bandwidth)
	red (668 nm center, 10 nm bandwidth)
	red edge (717 nm center, 10 nm bandwidth)
	NIR (840 nm center, 40 nm bandwidth)
RGB color output	Global shutter, aligned with all bands
Ground Sample Distance (GSD)	8 cm per pixel (per band) at 120 m
Capture Rate	1 capture per second (all bands), 12-bit RAW
Field of view	47.2° HFOV

4.3 Ground measurements

Ground measurements were conducted at the same time as the airborne data acquisition campaigns and included mid-day stem water potential using pressure chamber and proximal thermal imaging. Figure 10 shows the different locations where the measurements were taking place. In order to ensure spatial precision, each of the measurements was conducted in a known distance from the beginning of the row and its coordinates were registered using a GPS.

4.3.1 Mid-day stem water potential measurements

Mid-day stem water potential (Ψ_{stem}) was measured using a pressure chamber (Figure 7), model 3000F01 (Soil moisture Equipment Corp, Santa Barbara, CA, USA). Ψ_{stem} measurements provide information on the whole plant transpiration and root/soil hydraulic system (Chone et al., 2001; Williams et al., 2012). The measurements were conducted on three non- transpiring leaves (isolated by aluminum foil and nylon bag wrapping) per treatment (Figure 8).

Figure 7. The pressure chamber. Mid-day stem water potential (Ψ_{stem}) was measured at the same time as the airborne data acquisition campaigns, using a pressure chamber model 3000F01 pressure chamber. Ψ_{stem} measurements provide information on the whole plant transpiration and root/soil hydraulic system (photo: Alon Zuta).

Figure 8. Non-transpiring leaves. The Ψ_{stem} measurements were conducted on three non-transpiring leaves (isolated by aluminium foil and nylon bag wrapping) per treatment. (photo: Alon Zuta).

4.3.2 Proximal thermal imaging measurements

Proximal thermal images were taken during the airborne data acquisition campaigns to support the results obtained from the UAV and physiological measurements (Matese et al., 2018; Reshef et al., 2017) and were taken during the time of the UAV campaigns of August 22 and September 19. Infrared images were taken using an infrared thermal imaging camera (InfRec R500Pro, Nippon Avionics Co. Ltd., Tokyo, Japan) with a

resolution of 640×480 pixels and a temperature accuracy of ±1 °C, operating in the 8–14 µm waveband range, and equipped with an red, green and blue (RGB) acquisition imaging system. Images were taken at a distance of 1.5 m from the west and east facing sides of the canopy at the same locations of the stem water potential (Ψ_{stem}) measurements. Canopy emissivity was set at 0.98 as reported by Jones and Vaughan, (2010). Wet reference (T_{wet}) leaves were sprayed with water on both sides and dry reference leaves (T_{dry}) covered in petroleum jelly (Vaseline) on both sides to prevent transpiration as described by Jones, (1999 a) (Figure 9). The reference surfaces leaves were present in every image in order to exclude non-leaf material pixels during analyzing. Due to technical difficulties, the proximal thermal images of September 19 were taken only for the Ehrenfels vineyard. A radiometric calibration was periodically conducted in the laboratory using a blackbody. Additionally, ambient calibration which calculates compensation value on present ambient temperature, ambient humidity and distance was conducted in field.

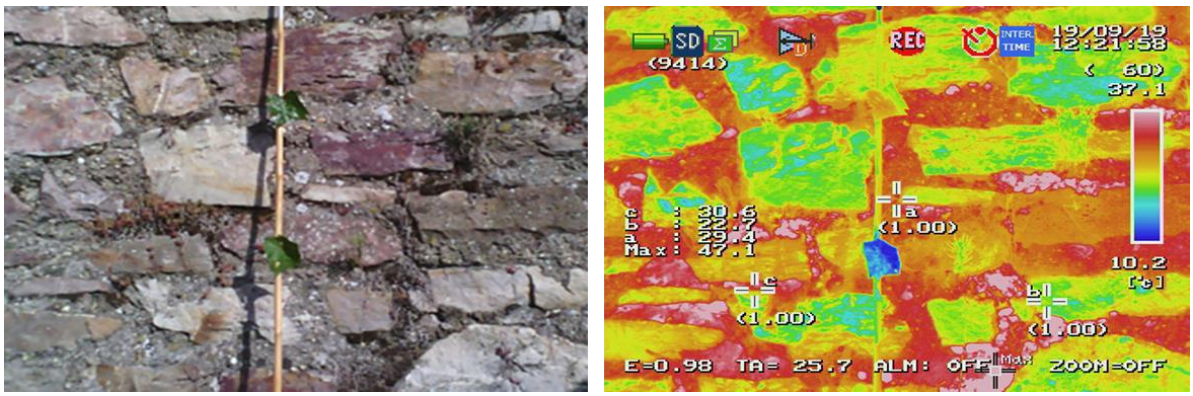

Figure 9. Reference surfaces for the proximal sensing. Left: reference surfaces for the proximal sensing measurements. Right: The references surfaces viewed by the thermal camera. (photo: Alon Zuta). The wet reference (T_{wet}) leaves (lower position on the stick) were sprayed with water on both sides and dry reference (T_{dry}) leaves (upper position on the stick) were covered in petroleum jelly (Vaseline) on both sides to prevent transpiration. The reference surfaces were used during the analysing process as threshold values to exclude non-leaf material pixels such as soil or sky.

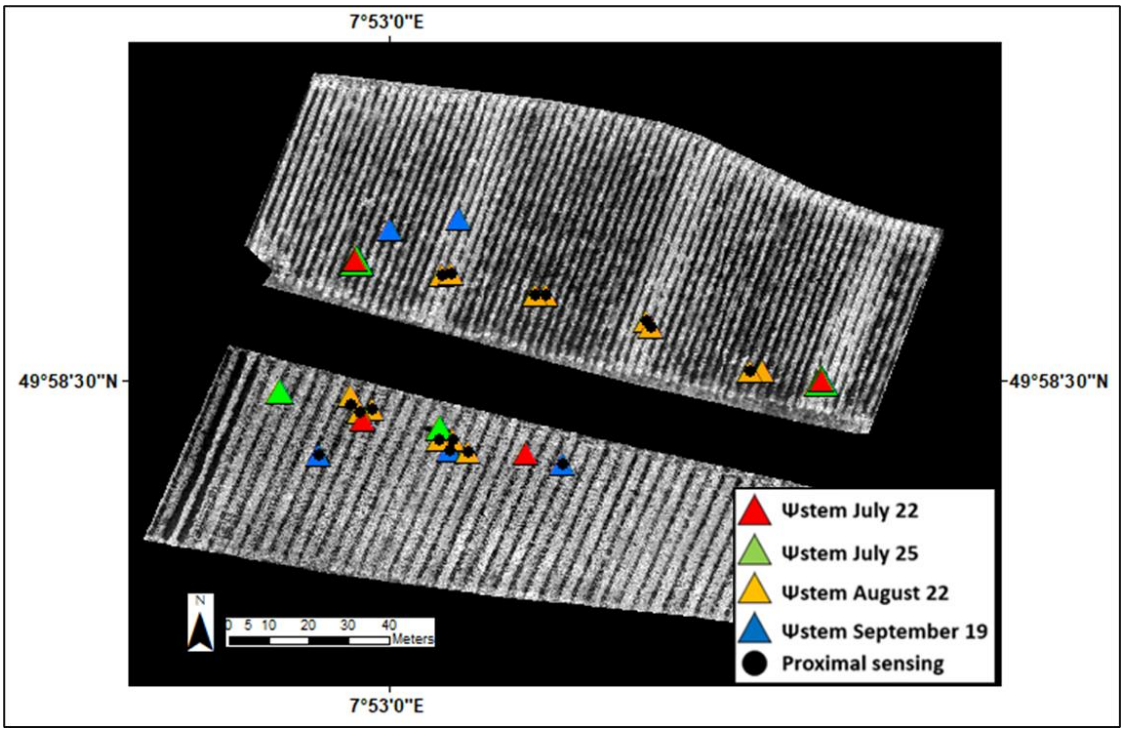

Figure 10. Location of ground measurements. The Figure shows the locations of the ground measurements (mid-day water potential and proximal thermal imaging) for the four measurement sessions.

4.3.3 Weather data

Weather data by intervals of 15 minutes (temperature, relative humidity, wind speed, wind direction, precipitation and global radiation) were acquired by the Ehrenfels weather station which is located on the southeastern corner of the Ehrenfels vineyard (Hochschule Geisenheim).

4.4 Airborne thermal data analysing

4.4.1 Initial data processing

T_{leaf} data in absolute temperature (C^o) were calculated from the thermal camera's digital number (DN) using an empirical line correction. The thermal imagery represents at-sensor radiance. Conversion was carried out during the flight campaigns using panels at known temperature as reference. The thermal images acquired by the UAV were mosaicked using Agisoft Photoscan Professional software (Agisoft LLC, St. Petersburg, Russia) which is capable of automatically going through sets of images, identifying features and aligned the images. The software is capable, as well, to generate and visualize a dense point cloud model. Based on the UAV positions from the GPS, the program calculates depth information for each pixel to be combined into a single dense 3D point cloud (Agisoft, 2019; Delgado Vera et al., 2017).

4.4.2 Grapevine pixel extraction

The 3D output from the Agisoft software allowed to develop a filtering procedure of the pure row pixels by subtracting known digital terrain model (DTM) from the resulting digital surface model (DSM) and later discriminating non grapevines by the global thresholding algorithm.

4.4.3 Cover crop pixel extraction

The same process described in section 4.4.2 was used to discriminate the grapevine's pixels. From the resulting image, the cover crop's pixels were extracted in two step process: The first step consisted of calculating normalized difference vegetation index (NDVI) which is a structural vegetation index utilized for the production of vigor maps (Matese et al., 2015) using the thermal and multispectral data bands obtained by the UAV. The NDVI was calculated as according to Rouse et al., (1973) as follows:

Eq. 1:
$$\mathrm{NDVI} = \frac{(\mathrm{NIR} - \mathrm{Red})}{(\mathrm{NIR} + \mathrm{Red})}$$

where near infrared (NIR) and red are the reflectance values in those respective bands of the electromagnetic spectrum (Hall et al., 2008). In the second step, in order to separate cover crop pixels from bare soil pixels, the bare soil pixels were discriminated through

setting a threshold value based on the values described in Montandon and Small, (2007) and comparison of the results to ground images of the cover crop which were taken for each row.

4.4.4 Thermal indices calculations

Both the crop water stress index (CWSI) and the stomatal conductance index (Ig) indices requires two baselines: a non-water stressed (T_{wet}) which represents a fully watered crop and a maximum water stressed (T_{dry}) which corresponds to a non-transpiring crop (Poblete Echeverría et al, 2017). For that purpose, a wet and dry 2 x 1 m polyester mesh surfaces (Figure 11) were placed in the experiment site during the UAV campaigns (Jones, 1999 b; Meron et al., 2013). The reference surface temperature was monitored using SI-111SS precision infrared radiometer (APOGEE Electronics, Santa Monica, CA, USA) connected to a CR300 data logger (Campbell Scientific INC, Logan, UT, USA). Due to failure of the wet surface to reach low enough temperature, only the values of the dry surface were used. The T_{wet} values were computed as the pixels with minimum value extracted within the studied vineyard on pure canopy pixels for grapevine-based analyses and pure cover crop for cover crop-based analyses as described at Alchanatis et al, (2010) and Baluja et al, (2012).

Figure 11. The reference surface temperature system. The 2X1m polyester mesh surfaces are monitored by a SI-111SS precision infrared radiometer connected to a CR300 data logger in order to provide minimum and maximum threshold temperatures for the analyses (photo: Alon Zuta).

Leaf radiometric temperature values acquired in the thermal infrared spectral region were used to calculate two thermal indices which are widely used as water status indicators: the crop water stress index (CWSI) (Idso et al., 1981) and the stomatal conductance index (Ig) (Jones, 1999a) as follows:

Eq. 2: $$CWSI = (Tcanopy - Twet) / (Tdry - Twet)$$

Eq. 3: $$Ig = (Tdry - Tcanopy) / (Tcanopy - Twet)$$

Where T_{canopy} (°C) is the canopy temperature obtained from the thermal images, and T_{wet} (°C) and T_{dry} (°C) are the lower and upper boundary reference temperature values, corresponding to a fully transpiring leaf with open stomata and non-transpiring leaf with closed stomata, respectively. The indices calculation was performed using ArcGIS 10.5.1 software (ESRI, Redlands, CA, USA).

4.4.5 Spatial interpolation

For each of the indices, an interpolated map was created in ArcGIS 10.5.1 software by using the following methods: Inverse Distance Weighting (IDW), Kriging, Local Polynomial, and Spline.

The inverse distance weighting or inverse distance weighted (IDW) method estimates the values of unsampled points based on a linear combination of values of the sampled points weighted by an inverse function of the distance from the point of interest to the sampled points. The assumption is that the values of the sampled points closer to the unsampled point are more similar to it than those further away (Li and Heap, 2008; Mitas and Mitasova, 2005; Setianto and Triandini, 2013) and is as follows:

Eq. 4:
$$Z_0 = \frac{\sum_{i=1}^{N} z_i \cdot d_i^{-n}}{\sum_{i=1}^{N} d_i^{-n}}$$

Where:

Z_0 = The estimation value of variable z in point I.

z_i = The sample value in point I.

d_i = The distance of sample point to estimated point.

N = The coefficient that determines weigh based on a distance.

n = The total number of predictions for each validation case.

Kriging, similar to IDW, weights the surrounding sample points to predict values for the unsampled locations but unlike IDW where the weights depend only on the distance, the weights also depend on the spatial relationships among the sampled points (Mitas and Mitasova, 2005; Setianto and Triandini, 2013):

Eq. 5:
$$Z(s_0) = \sum_{i=1}^{n} \lambda_i z(s_i)$$

Where:

$Z(s_i)$ = the sampled value at the ith location.

λ_i = an unknown weight for the sampled value at the ith location.

s_0 = the prediction location.

n = the number of measured values.

Local Polynomial interpolation computes a variety of polynomial equations to create a smooth surface that fits the neighbouring sampled points. The user can specify the neighbourhood's shape and number of points (ESRI, 2019 a).

Spline interpolation is a piecewise polynomial function which minimizes overall surface curvature, resulting in a smooth surface that passes exactly through the input points (Naoum and Tsanis, 2004).

4.4.6 Cross-validation

Evaluation of the resulting interpolated surfaces was conducted using cross-validation method available on ArcGIS. Cross-validation is a method of measuring the validity of the predictive ability of a model. It evaluates the output surfaces and produces error statistics describing the accuracy (Widman.T, 2011). It operates by removing each sampled point at a time and predicts the associated data value based on the rest of the sampled data and compares the measured values and predicted values. The procedure is repeated for all sampled points (Esri, 2019 b). The prediction errors for each interpolated surface was calculated based on the following Mean Error (ME) and Root Mean Square Error (RMSE) formulas (Zandi et al., 2011; Yao et al., 2013) as follows:

Eq. 6:
$$ME = \frac{1}{n}\sum_{i=1}^{n}\left[\hat{Z}(s_i) - z(s_i)\right]$$

Eq. 7:
$$RMSE = \sqrt{\frac{1}{n}\sum_{i=1}^{n}\left[\hat{Z}(s_i) - z(s_i)\right]^2}$$

Where:

Zˆ(si) = The interpolated (prediction) value.

z(si) = The measured actual value.

n = The number of validating points.

4.5. Proximal thermal imaging analysing

The proximal thermal images were analysed using a designated software (InfReC Analyzer Professional NS9500Pro). The reference surfaces were used during the analysing process as threshold values to exclude non-leaf material pixels such as soil or sky (Jones et al., 2002; Stoll and Jones, 2007). The temperature of each reference surface was calculated by aggregating and averaging the pixels within the polygons of each reference surface. The resulting values were used as threshold values in order to eliminate non-leaf material based on the assumption that any pixel value that was below or above the threshold values did not represent leaf material. The pixels of the image that did not fall between the reference values were eliminated and the remaining were aggregated and averaged to represent the overall temperature of the canopy (Figure. 12).

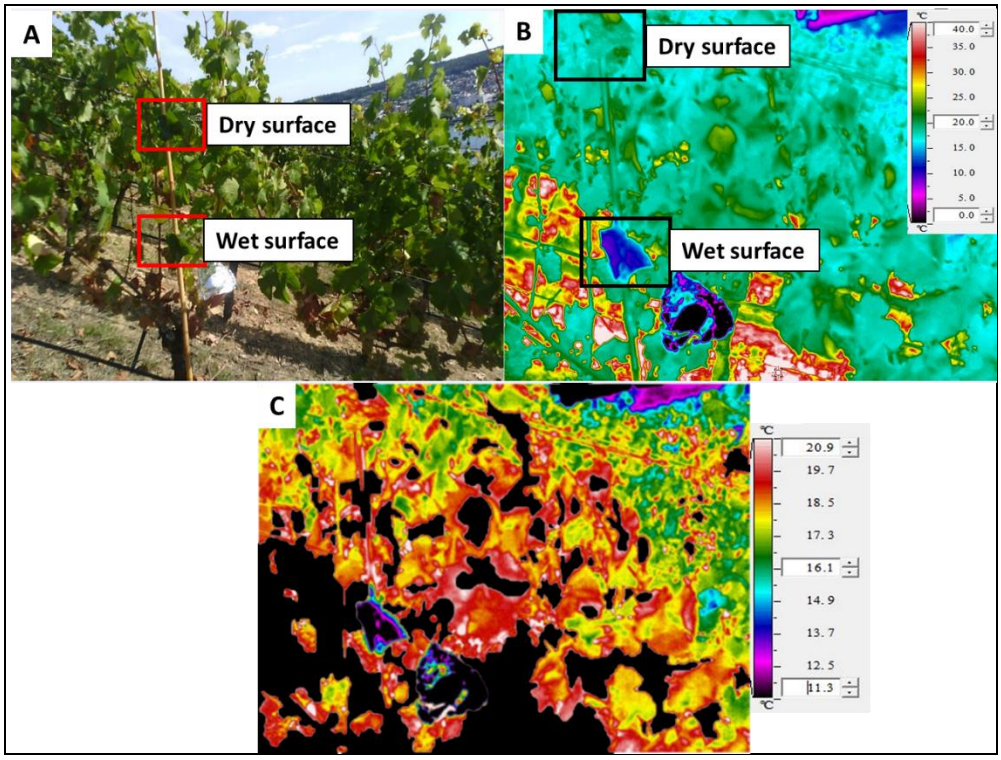

Figure 12. The process of removal of non-leaf material pixels. Image a. presents the grapevine canopy and the dry and wet reference surfaces. Image b. presents the grapevine canopy and the reference surfaces as perceived by the thermal camera. The temperatures of the reference surfaces were calculated by averaging the values of the pixels within the polygons of each reference surface. The resulting values were used as threshold values in order to eliminate non-leaf material based on the assumption that any pixel value that was below or above the threshold values did not represent leaf material. The result of the elimination process is seen in image c.

4.6 Comparison between ground measurements and interpolated surfaces

The values of the interpolated surfaces corresponding to the locations of the ground measurements were obtained using the Extract Values to Points tool of ArcGIS (Figure13) which extracts the cell values of a raster based on a set of point features and records the values in the attribute table.

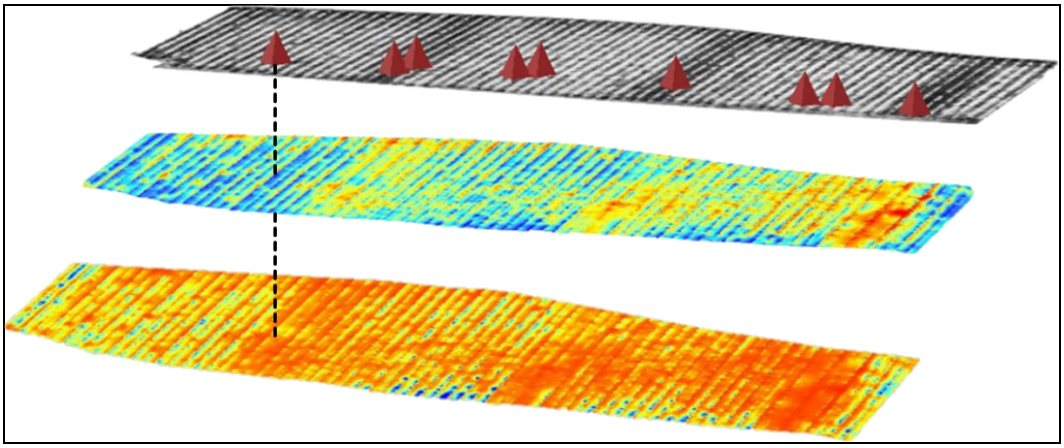

Figure 13. A graphic representation of Extract Values to Points tool. The locations of the ground measurements are placed on top of the interpolated surfaces. The pixel values of the different surfaces for each location are extracted into a table enabling the comparison between the ground measurement results and the interpolated surfaces through the calculation of the coefficient of determination.

5. Results

Figure 14 provides a visual description of the stages of producing interpolated surfaces. Figure14a shows the pixels captured by the UAV (marked green). Figure 14b shows the temperatures values for each of the pixels. Figures 14c and 14d show the interpolated surfaces for the CWSI and the Ig indices respectively. The resulting pattern of high-low values is similar to the pattern of irrigated and non irrigated regions of Figure 5. Table 5 shows the number of captured pixels for the grapevine canopy and the cover crop for each vineyard and measuring date and their percentage out of the total number of captured pixels (cover crop + grapevine) for the corresponding vineyard and date. It is noticeable that the number of captured cover crop pixels is, considerably, larger relatively to the number of captured grapevine pixels aside for the Burgweg measurements of September and August where the amount of grapevine canopy pixels is larger (marked yellow). Table 6 displays the results of the mid-day water stem (Ψ_{stem}) measurements obtained from the pressure chamber. Table 7 displays the results of the proximal thermal imaging after analyzed using the InfReC Analyzer software as described in section 4.5.

Table 5. Number of captured pixels. The table shows the number of captured pixels for the grapevine canopy and the cover crop for each vineyard and measurement date and their percentage out of the total number of captured pixels (cover crop + grapevine) for the corresponding vineyard and date.

Date	Vineyard	Number of cover crop pixels	Number of grapevine pixels	% of cover crop pixels out of the total	% of grapevine pixels out of the total
22-Jul	Bu	927,249	150,225	86.06	13.94
	Ef	1,240,869	90,085	93.23	6.77
25-Jul	Bu	592,589	163,082	78.42	21.58
	Ef	1,292,708	60,664	95.52	4.48
22-Aug	Bu	380,908	489,852	43.74	56.26
	Ef	1,007,425	126,112	88.87	11.13
19-Sep	Bu	308,508	418,909	42.41	57.59
	Ef	889,959	301,521	74.69	25.31

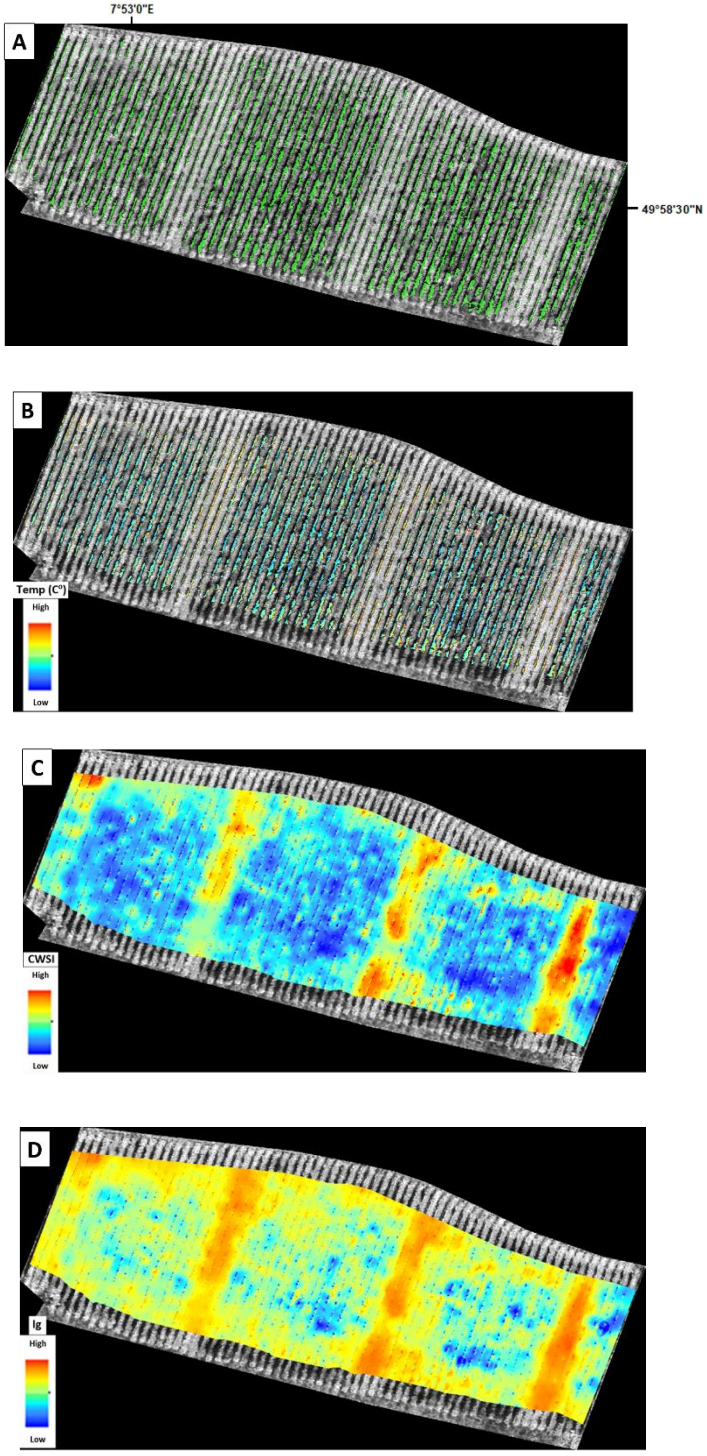

Figure 14. The processing of the UAV data. Figure 14a shows the pixels captured by the UAV system (marked green). Each pixel encompasses temperature value (figure 14b) which can be converted and interpolated to produce water status map of the entire vineyard. Figure 14c shows CWSI-based interpolated surface and figure 14d shows Ig-based interpolated surface.

Table 6. Results of the mid-day stem water potential measurements (Ψ_{stem}). The measurements were obtained using a pressure chamber. Ψ_{stem} measurements provide information on the whole plant transpiration and root/soil hydraulic system.

Date	Vineyard	result (bar)
22_07	BU	6.17
	BU	10.3
	Ef	6.88
	Ef	8.42
25_07	BU	6.75
	BU	10.27
	Ef	7.32
	Ef	9.92
22_08	BU	15.06
	BU	6.2
	BU	13.33
	BU	4.33
	Ef	12.4
	Ef	11.8
	Ef	11.6
	Ef	15
	Ef	15.6
	Ef	16.4
19_09	BU	22.2
	BU	19.5
	Ef	21.13
	Ef	17.7
	Ef	20.65

Table 7. Results of the proximal thermal imaging. The values were obtained by analyzing the thermal images in the InfReC Analyzer Professional NS9500Pro software (as described in section 4.5). For each of the measurements the following values are displayed: the wet reference surface temperature (T_{wet}), the dry surface temperature (T_{dry}), and the canopy of the canopy at the measured location (T_{canopy}).

Date	Vineyard	T_{wet}	T_{dry}	T_{canopy}
22/08	BU	21.52	29.43	29.12
	BU	21.35	28.42	27.08
	BU	19.16	27.57	23.57
	BU	20.16	28.45	24.28
	BU	18.02	29.36	25.81
	BU	19.03	29.46	27.32
	BU	15.90	25.79	22.93
	Eh	22.81	30.04	25.84
	Eh	21.11	30.33	26.19
	Eh	21.52	28.98	26.66
	Eh	20.31	29.19	25.64
	Eh	21.02	30.37	24.96
	Eh	21.69	30.59	27.16
19/09	Eh	13.29	24.71	19.00
	Eh	13.29	21.05	18.46
	Eh	11.69	21.75	17.57

5.1 Cross validation

The interpolated surfaces for each vineyard and date (for example, Burgweg July 22) were evaluated and compared based on their RMSE and ME results of the cross-validation analyzes similar to method described in Ohmer et al., 2017. Both the RMSE and the ME were assigned a rank value ranging from 1 to 16 since there are 16 interpolated surfaces for each vineyard-date combination. The smaller the error value, the lower the ranking value. The final ranking value was obtained by averaging the individual ranking values obtained for the RMSE and ME and, once more, re-ranking the results where the lower

the value, the better is the interpolated surface. The interpolated surfaces which achieved the lowest ranking value are considered to be the most fitting for their vineyard-date combination and are presented in table 8. All interpolated surfaces with their RMSE, ME and final ranking are presented in appendix 1, tables 1.1 -1.8.

Table 8. The best ranked interpolated surfaces based on the cross-validation results. The table shows the best interpolated surface for each vineyard-date combination. The interpolated surfaces were chosen based on the combined ranking of their ME and RMSE values.

Best Ranked Interpolated Surfaces Based on Cross-Validation Analyses					
Date	Vineyard	Interpolated Surface	ME	RMSE	Number of observations
22-Jul	Bu	Cover-CWSI-Local Polynomial	0.00018	0.027389	927,249
22-Jul	Ef	Cover-CWSI- Kriging	0.000272	0.000272	1,240,869
25-Jul	Bu	Cover-CWSI-Spline	0.0000934	0.016345	592,589
25-Jul	Ef	Cover-CWSI- Kriging	0.000133	0.042935	1,292,708
22-Aug	Bu	Vine-CWSI- Kriging	0.000413	0.024938	489,852
22-Aug	Ef	Cover-CWSI-Local Polynomial	0.00054	0.028361	1,007,425
19-Sep	Bu	Cover-CWSI-Spline	0.0000388	0.014367	308,508
19-Sep	Ef	Cover-CWSI-Spline	0.00019	0.014722	889,959

The results presented in table 8 show definite preference for cover crop and CWSI based interpolations. Seven out of eight of the highest ranked interpolated surfaces are cover crop based with only Burgweg, August 19 favoring grapevine based, and all are CWSI based. The table, as well, show a miscellany of interpolation algorithms which varies both spatially (between the two vineyards) and temporarily (between the different measurement dates).

5.2 Ground measurements

The interpolated surfaces were evaluated based on linear correlation and regression between them and the ground measurements data. The ranking of the interpolated surfaces is based on the coefficient of determination (R^2) of this relationship. The interpolated surfaces which received the highest R^2 values are considered to be the most fitting for their vineyard-date combination and are presented in tables 9 (correlation with Ψ_{stem}) and 10 (correlation with proximal thermal imaging). All interpolated surfaces with

their corresponding R^2 are presented in appendix 2, tables 2.1 -2.8 for the correlation with Ψ_{stem} and in appendix 3, tables 3.1-3.3 for the correlation with proximal thermal imaging. Due to the low number of collected points, the measurements of July 22 and 25 were converged into one dataset. This was decided to be feasible due to the proximity of the dates and similar weather conditions.

Table 9. The best ranked interpolated surfaces based on the Ψstem comparison. The table shows the best interpolated surface for each vineyard-date combination. The interpolated surfaces were chosen based on the coefficient of determination (R^2) results for the relationship between the mid-day water potential values (Ψ_{stem}) and the corresponding interpolated method which achieved by the extract values to point procedure.

Best Ranked Mid-day Ψstem -Interpolation Comparison			
Date	Vineyard	Interpolated Surface	R^2
July	Bu	Cover-Ig-Spline	0.967
July	Ef	Cover-Ig-IDW	0.679
22-Aug	Bu	Vine-Ig-Local Polynomial	0.881
22-Aug	Ef	Vine-Ig-IDW	0.895
19-Sep	Bu	Vine-CWSI-IDW	0.967
19-Sep	Ef	Vine-Ig-IDW	0.998

Table 10. The best ranked interpolated surfaces based on the proximal thermal imaging comparison. The table shows the best interpolated surface for each vineyard-date combination. The interpolated surfaces were chosen based on the coefficient of determination (R^2) results for the relationship between the proximal thermal imaging and the corresponding interpolated method which achieved by the extract values to point procedure.

Best Ranked Proximal Sensitivity-Interpolation Comparisons			
Date	Vineyard	Interpolated Surface	R^2
22-Aug	Bu	Vine-Ig-Local Polynomial	0.702
22-Aug	Ef	Cover-Ig-Local Polynomial	0.997
19-Sep	Ef	Cover-Ig-Spline	0.999

Both the Ψ_{stem} and the proximal thermal imaging comparisons show preference to Ig-based methods. Five out of the six Ψ_{stem} to interpolation comparison summary results are Ig based and only one is CWSI based. All three proximal thermal imaging to interpolation comparison summary results are Ig based. The Ψ_{stem} to interpolation summary results show that the highest ranked interpolated surfaces for the July measurements are cover crop-based for both vineyards while the highest ranked interpolated surfaces for the August and September measurements are grapevine-based for both vineyards. The

proximal thermal imaging to interpolation results show that two out of three favor cover crop-based interpolation. The results, both for Ψ_{stem} and proximal thermal imaging exhibit miscellany of interpolation algorithms which varies both spatially (between the two vineyards) and temporarily (between the different measurement dates).

6. Discussion

6.1 Comparison of interpolation methods

The performance of an interpolation algorithm depends on the nature and quality of the data including factors such as sample density, sample spatial distribution, sample clustering, surface type, data variance, data normality, resolution, and the interactions between the factors (Li and Heap, 2011). Different interpolation methods are data and variable specific (Li and Heap, 2008) and act differently with different input. Therefore, under various circumstances, the same methods will operate in different levels of success.

The results show that there is no single interpolation method that fits both vineyards, both crop type (cover and grapevine) and all measurement dates. A striking observation is the difference in results between the two vineyards. Even though Burgweg and Ehrenfel are located in great proximity (less than 15 meters), share the same type of grapevine and same row orientation towards the sun, their slight changes in setup such as row width and planting density (table 2) led to different resulted interpolated surfaces.

A second observation is the difference in results between the different measurement dates. As the airborne thermal data collection is based on radiation emitted from the leaves, changes in density, distribution and surface area affect the quality of the data. Therefore, the changes in the number of captured pixels noted in table 5 resulted in different interpolation surfaces showing different fitness levels for the measurement dates. These changes can be attributed to the development of the grapevine canopy and changes in extant of the cover crop during the growing season (Munitz et al., 2016 a; Munitz et al., 2016 b; Skrotch and Shribbs, 1986).

6.2 Comparison of indices

The comparisons between the interpolated surfaces and the ground measurements exhibit preference of Ig-based interpolation surfaces which corresponds to the assumption that Ig index is more suitable to the climate of the Rheingau region. The results of the cross validation, on the other hand, show preference of CWSI-based interpolation surfaces. The preference of CWSI over Ig in the cross-validation results can be attributed to the range of potential values rather than the suitability of the indices. CWSI has definite possibilities of values that can only range from 0 (no water stress) to 1 (maximum water

stress) while the Ig index is proportional to stomatal conductance and, theoretically, has an infinite set of potential values (Idso et al., 1981; Jones, 1999a). Although in the current research project, a threshold was set in a way that interpolated values cannot exceed the min and max values of T_{dry} and T_{wet}, the range of values of Ig-based interpolation was, still, considerably bigger than that of CWSI-based interpolation.

6.3 Comparison of crop type

As sample size and distribution increases accuracy (Kravchenko, 2003; Widman, 2011), cover crop-based methods show an advantage in the cross-validation analyses due to their large number of captured pixels relatively to the grapevine canopy. The single interpolated surface – proximal thermal imaging comparison which favors grapevine (Burgweg, August) can be attributed to the lower number of cover crop pixels and the higher number of grapevine canopy pixels for the Burgweg vineyard for that measuring date (table 5).

The Ψstem to interpolation summary results show that the best ranked interpolated surfaces for the July measurements are cover crop-based for both vineyards while the best ranked interpolated surfaces for the August and September measurements are grapevine-based for both vineyards. This can be the result of a fault in the Ψstem procedure which is further discussed in section 6.5.

6.4 Suitability of cover crop-based interpolation for other types of environments

Grapevines and cover crops compete over resources including soil moisture (Celette et al, 2008). Cover crops begin to take up water before grapevine budbreak and can dry out the surrounding soil compartment before grapevine plants can sufficiently uptake water. This leads to the grapevine modifying its rooting structure and exploring deeper soil layers, resulting in different soil zones being exploited by the different species and limits the competition (Morlat and Jacquet, 2003). This phenomenon is possible in deep soils vineyards. As the current research project was conducted in steep sloped vineyards characterized by shallow stony soils less than 1.5 m in depth (Hofmann et al., 2014), the root distribution was limited. It is evident by the findings of this research project that both the cover crop and the grapevines were affected by the water distribution in a similar way. As such, use of cover crop as an indicator of water stress is a viable option for

monitoring water status in vineyards. However, further research would be beneficial to determine if use of cover crops could be performed for water stress analysis in vineyards with deeper soil layers such as those in flat regions.

6.5 Ground measurements limitation

Although the current research highlighted the importance in defining a suitable interpolation method, the main limitation of this research study is its reliance on ground measurements for validation. Both stem water potential and ground based thermal imaging which are used to validate the data gathered by the UAV are highly time-consuming methods resulting in small sample size, especially as they have to be conducted during the same timeframe as the airborne images are being taken. Stem water potential measurement using pressure chamber is, significantly, slow procedure which yields small sample size as it can only sample one leaf per measurement. Additionally, its accuracy is greatly affected by the operator, especially when determining the endpoint (Levin, 2019; Suter et al, 2019), potentially, leading to inaccurate measurements. Proximal thermal imaging has a few advantages over pressure chamber measurements as it less susceptible to operator error and can capture larger volume of data over larger sections of the canopy.

6.6 The use of reference surfaces for proximal thermal imagery

The design of a threshold values method which can be both accurate and easily computed during the aerial thermal imagery acquisition is a complexed task as the choice of reference may affect the value of the mean temperature and the frequency distribution of temperatures obtained (Jones et al, 2002).

The use of wet and dry reference surfaces as thresholds to determine limits of the canopy temperature distribution was proposed by Jones 1999a which also concluded that real leaves (either sprayed with water or covered in petroleum jelly) provided the best references because of their similar properties to the canopy being studied.

A major limitation of the use of references surfaces is that in cases where the stomata is very open or very closed, the temperature of the canopy might be similar to the temperature of the reference surface leading to the exclusion of canopy pixels (Leinonen and Jones, 2004).

Additional limitation is that the non-leaf objects such as stems or ground that their temperature range falls between the references might be included in the analysing (Leinonen and Jones, 2004).

7. Conclusion

The aim of the current research project was to evaluate different aspects of mapping water stress in vineyards using the technique of airborne thermal Imaging. The study demonstrated the advantages of using cover crop data over grapevine based airborne thermal data for assessing the vineyard water stress in steep slope vineyards. Additionally, the current study demonstrated how temporal and spatial changes affect the distribution of sample points and as result, influence the suitability of different interpolation algorithms. Consequently, the importance of selecting the most appropriate interpolation algorithm has been shown to be of upmost importance in mapping of water stress for agricultural crops. Finally, it was established that the Jones stomatal conductance index (Ig) is more suitable than the crop water stress index (CWSI) for mapping water stress index in regions with climatic variability and high humidity such as the Rheingau, Germany.

The current study highlighted several important considerations and implications in measuring and mapping the spatial and temporal crop water stress in vineyards which will assist future research on further development of the technique.

The combination of thermal sensors and unmanned aerial vehicles technologies provides an opportunity for monitoring water stress in crop fields and a method to improve irrigation management. The rapid improvement of these technologies, the considerable reduction in cost, and the evolvement of open source electronic community have the potential to enable this tool to be available for use for any winegrowers and, consequently, lead to both reduction in irrigation costs and more sustainable use of water which is a vital necessity in the current context of climate change and water scarcity. With that, further studies should be conducted on the cost effectiveness of thermal-based irrigation management in commercial scales.

References

Adhikary, P.P., and C.J. Dash. 2014. Comparison of deterministic and stochastic methods to predict spatial variation of groundwater depth. *Applied Water Science* 7:339–348, doi: 10.1007/s13201-014-0249-8

Agisoft, Metashape User Manual. 2019. Retrieved December 20, 2019, from https://www.agisoft.com/downloads/user-manuals/

Aguilar, F. J., F. Aguera, M.A. Aguilar, F. Carvajal. 2005. Effects of terrain morphology, sampling density, and interpolation methods on grid DEM accuracy. *Photogrammetric Engineering and Remote Sensing* 71: 805–816. doi: 10.14358/PERS.71.7.805.

Alchanatis, V., Y. Cohen, S. Cohen, M. Moller, M. Sprinstin, M. Meron, J. Tsipris, Y. Saranga, E. Sela. 2010. Evaluation of different approaches for estimating and mapping crop water status in cotton with thermal imaging. *Precision Agriculture*. doi: 10.1007/s11119-009-9111-

Alchetron, Rüdesheim and Assmannshausen vineyards. Retrieved: October 28, 2019, from https://alchetron.com/Rheingau-(wine-region)

Baert, A., K. Villez, K. Steppe. 2013. Automatic drought stress detection in grapevines without using conventional threshold values. *Plant and Soil* 369(1-2): 439-452. doi: 10.1007/s11104-013-1588-1

Baluja, J., M.P Diago, P. Balda, R. Zorer, F. Meggio, F. Morales, J. Tardaguila. 2012. Assessment of vineyard water status variability by thermal and multispectral imagery using an unmanned aerial vehicle (UAV). *Irrigation Science* 30: 511-522. doi: 10.1007/s00271012-0382-9

Bardedo, A. 2019. A Review on the Use of Unmanned Aerial Vehicles and Imaging Sensors for Monitoring and Assessing Plant Stresses. *Drones* 3(2). doi: 10.3390/drones3020040.

Bellvert, J., P.J Zarco-Tejada, J. Girona, E. Fereres. 2013. Mapping Crop Water Stress Index in a 'Pinot-Noir Vineyard: Comparing Ground Measurements with Thermal Remote Sensing Imagery from an Unmanned Aerial Vehicle. Precision *Agriculture* 15(4): 361-376. doi: 10.1007/s11119-013-9334-5

Bellvert, J., J. Marsal, J. Girona J, P.J. Zarco-Tejada. 2014. Seasonal evolution of crop water stress index in grapevine varieties determined with high-resolution remote sensing thermal imagery. *Irrigation Science*. 33: 81–93. doi: 10.1007/s00271-014-0456-y

Bellvert, J., P.J Zarco-Tejada, J. Marsal, J. Giron, V. Gonzales-Dugo, E. Fereres. 2015. Vineyard irrigation scheduling based on airborne thermal imagery and water potential thresholds, Australian Society of Viticulture and Oenology Inc, doi: 10.1111/ajgw.12173

Ben Gal, A., N. Agam, V. Alchanatis, Y. Cohen, U. Yermiyahu, I. Zipori, E. Presnov, M. Sprintsin, A. Dag. 2009. Evaluating water stress in irrigated olives: correlation of soil water status, tree water status, and thermal imagery. *Irrigation Science*, doi: 10.1007/s00271-009-0150-7

Berni, J., P. Zarco-Tejada, L. Suárez, E. Fereres. 2009. Thermal and Narrowband Multispectral Remote Sensing for Vegetation Monitoring from an Unmanned Aerial Vehicle. *IEEE Transactions on Geoscience and Remote Sensing* 47(3): 722-738. doi: 10.1109/TGRS.2008.2010457

Blanco-Cipollone, F., S. Lourenço, J. Silvestre, N. Conceição, M.J. Moñino, A. Vivas, M.I. Ferreira

.2017. Plant Water Status Indicators for Irrigation Scheduling Associated with Iso- and Anisohydric Behavior: Vine and Plum Trees, *Horticulturae* 3 (47). doi:10.3390/horticulturae3030047.

Bockhold, D.L., A.L. Thompson, K.A. Sudduth, J.C Henggeler. 2011. Irrigation Scheduling Based on Crop Canopy Temperature for Humid Environments. *American Society of Agricultural and Biological Engineers* 54(6): 2021-2028. doi: 10.13031/2013.40654

Celette, F., R. Gaudin, G. Christian. 2008. Spatial and temporal changes to the water regime of a Mediterranean vineyard due to the adoption of cover cropping, *European Journal of Agronomy* 29(4): 153-162. doi: 10.1016/j.eja.2008.04.007

Chone, X., C. van Leeuwen, D. Dubourdieu, J.P Gaudillère. 2001. Stem Water Potential is a Sensitive Indicator of Grapevine Water Status, *Annals of Botany* (87): 477-483. doi: 10.1006/anbo.2000.1361

CIA Factbook, map of Germany, retrieved: October 28, 2019 from https://www.cia.gov/library/publications/the-world-factbook/geos/gm.html

Costa, J.M., M.F. Ortuno, C.M Lopes, M.M Chaves. 2012. Grapevine varieties exhibiting differences in stomatal response to water deficit. *Functional Plant Biology* 39(3): 179-189 doi: 10.1071/FP11156

Curtarelli, M., J. Leão, I. Ogashawara, J. Lorenzzetti, J. Stech. 2015. Assessment of Spatial Interpolation Methods to Map the Bathymetry of an Amazonian Hydroelectric Reservoir to Aid in Decision Making for Water Management. *International Journal of Geo-Information* 4: 220-235. doi: 10.3390/ijgi4010220

Delgado-Vera, C., M. Aguirre-Munizaga, M. Jiménez-Icaza, N. Manobanda-Herrera, A. Rodríguez-Méndez. 2017. A Photogrammetry Software as a Toolfor Precision Agriculture: A Case Study. Technologies and Innovation: Third International Conference, Guayaquil, Ecuador. doi: 10.1007/978-3-319-67283-0_21

Diago, M.P., A. Bellincontro, M. Scheidweiler, J. Tardaguila, S. Tittmann, M. Stoll. 2017. Future Opportunities of Proximal Near Infrared Spectroscopy Approaches to Determine the Variability of Vineyard Water Status: Near Infrared Spectroscopy to Assess Vine Water Status, *Australian Society of Viticulture and Oenology Inc*. doi: 10.1111/ajgw.12283

Esri, 2019 a, how local polynomial interpolation works, retrieved on October 19, 2019 from https://pro.arcgis.com/en/pro-app/help/analysis/geostatistical-analyst/how-local-polynomial-interpolation-works.htm

Esri b. 2019. Performing Cross-Validation and Validation. Retrieved on October 19, 2019 from https://desktop.arcgis.com/en/arcmap/latest/extensions/geostatistical-analyst/performing-cross-validation-and-validation.htm,

Fraga, H., I.G de Cortázar Atauri, A.C Malheiro A.C, J.A Santos. 2016. Modelling climate change impacts on viticultural yield, phenology and stress conditions in Europe. *Global Change Biology* 22(11): 3774-3788, doi:10.1111/gcb.13382

Fuentes, S., R. De Bei, J. Pech, S. Tyerman. 2012. Computational water stress indices obtained from thermal image analysis of grapevine canopies, *Irrigation Science*, doi: 10.1007/s00271-012-0375-8

Gates, D.M. 1964. Leaf temperature and transpiration. *Agronomy Journal* 56: 273–277

Google, Rüdesheim am Rhein, retrieved on October 28, 2019 from https://www.google.com/maps/place/65385+R%C3%BCdesheim+am+Rhein/@50.0288887,7.8230782,23764m/data=!3m1!1e3!4m5!3m4!1s0x47bde6300d8c792b:0x422435029b0a270!8m2!3d49.9821443!4d7.9301124

Grant, O.M., M.M. Chaves M.M, H.G. Jones. 2006. Optimizing thermal imaging as a technique for detecting stomatal closure induced by drought stress under greenhouse conditions, *Physiologia Plantarum* 127: 507–518. doi: 10.1111/j.1399-3054.2006.00686.x,

Grant, O.M., H. Ochagavía, J. Baluja, M.P. Diago, J. Tardáguila. 2016. Thermal imaging to detect spatial and temporal variation in the water status of grapevine (Vitis vinifera L.). *The Journal of Horticultural Science and Biotechnology* 91(1): 43-54, doi: 10.1080/14620316.2015.1110991

Gruber, B., and H.R Schultz. 2005. Water relations of grapevines in steep slope viticulture. GESCO Proceedings, Geisenheim, Germany.

Gutiérrez, S., M.P Diago, J. Fernández-Novales, J. Tardaguila. 2018. Vineyard Water Status Assessment Using On-The-Go Thermal Imaging and Machine Learning. *PloseOne* 13(2). doi: 10.1371/journal.pone.0192037

Hall, A., J.P Louis J.P, D.W Lamb. 2008. Low-resolution remotely sensed images of Winegrape vineyards map spatial variability in planimetric canopy area instead of leaf area index. *Australian Journal of Grape and Wine Research* 14: 9–17. doi: 10.1111/j.1755-0238.2008.00002.x

Hannah, L., P.R Roehrdanz, M. Ikegami, A.V Shepard, M.R Shaw, G. Tabor, L. Zhi, P.A Marquet, R.J Hijmans. 2013. Climate change, wine, and conservation, *Proceedings of the National. Academy of Sciences of the USA* 110: 6907–6912. doi: 10.1073/pnas.1210127110

Hochschule Geisenheim, Tagesauswertungen der Wetterstationen, retrieved on October 20, 2019 from http://rebschutz.hs-geisenheim.de/wetterstationen/tagesauswertung.php

Hofmann, M., R. Lux, H.R Schultz. 2014. Constructing a framework for risk analyses of climate change effects of the water budget of differently sloped vineyards with a numeric simulation using the Monte Carlo method coupled to a water balance mode., *Frontiers in Plant Sciences* 5: 1-22. doi: 10.3389/fpls.2014.0064

Hofmann, M., and H.R Schultz. 2015. Modeling the water balance of sloped vineyards under various climate change scenarios. BIO Web of Conferences 5. doi: 10.1051/bioconf/20150501026.

Hofmann, H., R. Jensen, A. Thomsen, H. Nieto. 2016. Crop Water Stress Maps for Entire Growing Seasons from Visible and Thermal UAV imagery. *Biogeosciences Discussion* 10. doi: 10.5194/bg-2016-316.

Hruska, R., J. Mitchell, M. Anderson, N.F Glen. 2012. Radiometric and Geometric Analysis of Hyperspectral Imagery Acquired from an Unmanned Aerial Vehicle. *Remote Sensing* 4: 2736-2752. doi:10.3390/rs4092736.

Idso, S.B., R.D Jackson, P.J Pinter, R.J Reginato, J.L Hatfield. 1981. Normalizing the Stress Degree- Day Parameter for Environmental Variability. *Agricultural and Forest Meteorology* 24:45–55. doi: 10.1016/0002-1571(81)90032-7.

Idso, S.B. 1982. Non-water-stressed baselines: A key to measuring and interpreting plant water stress. *Agricultural Meteorology* 27(1-2): 59-70. doi: /10.1016/0002-1571(82)90020-6

Jackson, R.D. 1982. Canopy Temperature and Crop Water Stress, *Advances in Irrigation* 1: 43-85. doi: 10.1016/B978-0-12-024301-3.50009-5

Jones, H.G. 1990. Plant water relations and implications for irrigation scheduling, *Acta Horticulturae* 278: 67–76.

Jones, H.G., D. Aikman D, T.A. Mcburney. 1997. Improvements to Infra-red Thermometry for Irrigation scheduling in Humid Climates. *ISHS Acta Horticulture* 449. doi: 10.17660/ActaHortic.1997.449.37

Jones#, H.G. 1999 (a). Use of Infrared Thermometry for Estimation of Stomatal Conductance as a Possible Aid to Irrigation Scheduling. *Agricultural and Forest Meteorology* 95:139–149. doi: 1016/S0168-1923(99)00030-1

Jones, H.G. 1999 (b). Use of thermography for quantitative studies of spatial and temporal variation of stomatal conductance over leaf surfaces. *Plant Cell and Environment* 22: 1043-1055

Jones, H.G., M. Stoll, T. Santos, C. de Sousa, M.M. Chaves, O.M Grant. 2002. Use of infrared thermography for monitoring stomatal closure in the field: application to grapevine. *Journal of Experimental Botany* 53(378): 2249–2260. doi: 10.1093/jxb/erf083

Jones, H.G. 2004 (a). Application of Thermal Imaging and Infrared Sensing in Plant Physiology and Ecophysiology. *Advances in Botanical Research* 41: 107-163. doi: 10.1016/S0065-2296(04)41003-9

Jones, H.G. 2004 (b). Irrigation scheduling: advantages and pitfalls of plant-based methods. *Journal of experimental botany* 55(407): 2427–2436. doi: 10.1093/jxb/erh213 PMID: 15286143

Kottek, M., J. Grieser, C. Beck, B. Rudolf, F. Rubel. 2006. World Map of the KöppenGeiger climate classification updated. *Meteorologische Zeitschrift* 15 (3): 259-26

Kravchenko, A.N. 2003, Influence of Spatial Structure on Accuracy of Interpolation Methods. *Soil Science of America* 67 (5): 1564-1571. doi:10.2136/sssaj2003.1564.

Leinonen, I., and H.G Jones. 2004. Combining thermal and visible imagery for estimating canopy temperature and identifying plant stress. *Journal of Experimental Botany* 55: 1423–1431. doi: 10.1093/jxb/erh146.

Levin, A.D. 2019. Re-evaluating pressure chamber methods of water status determination in field-grown grapevine (vitis spp), *Agricultural Water Management* 221: 422-429. doi: 10.1016/j.agwat.2019.03.026

Li, J., and A.D. Heap. 2008. A Review of Spatial Interpolation Methods for Environmental Scientists, Geoscience Australia, Canberra Australia.

Li, J., and A.D Heap. 2011. A review of comparative studies of spatial interpolation methods in environmental sciences: Performance and impact factors. *Ecological Informatics* 6: 228-241. doi: doi.org/10.1016/j.ecoinf.2010.12.003

Lopes, C., A. Monteiro, F.E. Ruckert, B. Gruber, B. Steinberg, H.R. Schultz. 2004. Transpiration of grapevines and co-habitating cover crop and weed species in a vineyard. A "snapshot" at diurnal trends. *Vits* 43(2): 111-117

Lopes, C.M. 2016. Cover Crops Competition for Water in Vineyards: Case Studies in Mediterranean Terroirs. 11th International Terroir Congress, McMinnville, Oregon, USA.

Matese, A., P. Toscano, S.F Di Gennaro, L. Genesio, F.P. Vaccari, J. Primicerio, C. Belli, A. Zaledi, R. Bianconi, B. Gioli. 2015. Intercomparing of UAV, Aircraft and Satellite Remote Sensing Platforms for Precision Viticulture. *Remote Sensing* 7: 2971-2990. doi:10.3390/rs70302971

Matese, A., R. Baraldi, A. Berton, C. Cesaraccio, S.F. Di Gennaro, P. Duce, O. Facini, M.G. Mameli, A. Piga, A. Zaldei. 2018. Estimation of Water Stress in Grapevines Using Proximal and Remote Sensing Methods. *Remote Sensing* 10 (114). doi: 10.3390/rs10010114

McCutchan, H., and K.A. Shackel. 1992. Stem-water Potential as a Sensitive Indicator of Water Stress in Prune Trees (Prunus domestica L.cv. French). *Journal of the American Society for Horticultural Science* 117(4): 607-611

Meron, M., M. Sprintsin, J. Tsipris, V. Alchanatis, Y. Cohen. 2009. Canopy temperature interpretation of thermal imagery for crop water stress determination. 7th European Conference on Precision Agriculture

Meron, M, M. Sprintsin, J. Tsipris, V. Alchanatis, Y. Cohen. 2013. Foliage temperature extraction from thermal imagery for crop water stress determination. *Precision Agriculture* 14 (5). doi: 10.1007/s11119-013-9310-0,

Montandon, L.M., and E.E. Small. 2007. The impact of soil reflectance on the quantification of the green vegetation fraction from NDVI. *Remote Sensing of Environment* 112 (4): 1835-1845. doi: 10.1016/j.rse.2007.09.007

Monteith, J. L., and G. Szeicz. 1962. Radiative temperature in the heat balance of natural surfaces. *Quart Journal Royal. Meteorological Society* 88: 496-507. doi: 10.1002/qj.4970883781

Monteiro, A., and C.M. Lopes. 2006. Influence of cover crop on water use and performance of vineyard in Mediterranean Portugal. *Agriculture, Ecosystems & Environment* 121(4): 336-342. doi: 10.1016/j.agee.2006.11.016.

Morlat, R., and A. Jacquet. 2003. Grapevine Root System and Soil Characteristics in a Vineyard Maintained Long-term with or without Interrow Sward. *American Journal of Enology and Viticulture* 54:1-7

Mitas, L., and H. Mitasova. 2005. Spatial Interpolation. In: Longley., P.A. Goodchild, M.F. Maguire D.W. Eds., Geographic Information Systems: Principles, Techniques, Management and Applications, 2nd Edition, Vol. 1, Part 2, Chapter 34.

Munitz, S., A. Schwartz, Y. Netzer. 2016 (a). Evaluation of Seasonal Water Use and Crop Coefficients for Cabernet Sauvignon' grapevines as the base for skilled regulated deficit irrigation. *Acta Horticulturae*. doi: 10.17660/ActaHortic.2016.1115.6.

Munitz, S., A. Schwartz, Y. Netzer. 2016 (b). Sustained and Regulated Deficit Irrigation of Field-Grown Merlot Grapevines. *Australian Journal of Grape and Wine Research*. doi: 10.1111/ajgw.12241

Naoum, S., and I.K. Tsanis. 2004. Ranking spatial interpolation techniques using a GIS-based DSS. *Global NEST Journal* 6(1). doi: 10.30955/gnj.000224

Novara, A., L. Gristina, F. Guaitoli, A. Santoro, A. Cerda. 2013. Managing soil nitrate with cover crops and buffer strips in Sicilian vineyards. *Solid Earth* 4: 255-262. doi: 10.5194/se-4-255-2013.

Ohmer, M., T. Liesch, N. Goepprt, N. Goldschieder. 2017. On the optimal selection of interpolation methods for groundwater contouring: an example of propagation of uncertainty regarding inter-aquifer exchange. *Advances in Water Resources* 109: 121-132. doi: 10.1016/j.advwatres.2017.08.016

Pirasteh-Anosheh, H., A. Saed-Moucheshi, H. Pakniyat, M. Pessarakli. 2016. Stomatal responses to drought stress. *Water Stress and Crop Plants*. doi: 10.1002/9781119054450.ch3

Poblete-Echeverría, C., D. Espinace, D. Sepúlveda-Reyes, M. Zúñiga, M. Sanchez. 2017. Analysis of crop water stress index (CWSI) for estimating stem water potential in grapevines: comparison between natural reference and baseline approaches. *Acta horticulturae* 1150: 189-194. doi: 10.17660/ActaHortic.2017.1150.27

Pou, A., M.P. Diago, H. Medrano, J. Baluja, J. Tardaguila. 2013. Validation of thermal indices for water status identification in grapevine. *Agricultural Water Management* 134: 60-72. doi: 10.1016/j.agwat.2013.11.010

Reshef, N., N. Walbaum, N. Agam, A. Fait. 2017. Sunlight Modulates Fruit Metabolic Profile and Shapes the Spatial Pattern of Compound Accumulation within the Grape Cluster. *Frontiers in Plant Science* 80: 1-20. doi: 10.3389/fpls.2017.00070.

Rodrigues, M.S., D.C. Alves, V.C de Souza, A.C. de Melo, A.M. Nascimento Lima, J.C. Cunha. 2018. Spatial interpolation techniques for site-specific irrigation management in a mango orchard. *Comunicata Scientiae* 9(1): 93-101. doi: 10.14295/CS.v9i1.2645

Robinson, T.P., and G. Metternicht. 2006. Testing the performance of spatial interpolation techniques for mapping soil properties. *Computers and Electronics in Agriculture* 50: 97-108. doi: 10.1016/j.compag.2005.07.003

Rouse, J.W., R.H. Haas, J.A. Schell, D.W. Deering. 1973. Monitoring vegetation systems in the Great Plains with ERTS. Proceedings of the Third ERTS Symposium,Washington, DC, USA.

Ruiz-Colmenero, M., R. Bienes, D.J. Eldridge, M.J. Marques. 2012. Vegetation cover reduces erosion and enhances soil organic carbon in a vineyard in the central Spain. *Catena* 104: 153-160. doi: 10.1016/j.catena.2012.11.007.

Santesteban, L.G., S.F. Di Gennaro, A. Herrero-Langero, C. Miranda, J.B. Royo J.B, A. Matese. 2017. High resolution UAV-based thermal imaging to estimate the instantaneous and seasonal variability of plant water status within a vineyard. *Agricultural Water Management* 183: 49-59.doi: 10.1016/j.agwat.2016.08.026

Schultz, H.R., and M. Stoll. 2010. Some critical issues in environmental physiology of grapevines: future challenges and current limitations. *Australian Journal of Grape and Wine Research* 16: 4–24

Setianto, A., and T. Triandini. 2013. Comparison of Kringing and Inverse Distance weigheted (IDW) Interpolation Methods in Lineament Extraction and Analysis. *Journal of Applied Geology* 5(1). doi: 10.22146/jag.7204.

Simonneau, T., E. Lebon, A. Coupel-Ledru, E. Marguerit, L. Rossdeutsch, N. Ollat. 2017. Adapting plant material to face water stress in vineyards: which physiological targets for an optimal control of plant water status? *Oenone* 51(2). doi:.org/10.20870/oeno-one.2017.51.2.1870.

Skrotch, W., and J.M. Shribbs. 1986. Orchard floor management: an overview. *Hortscience* 21: 390-394

Steenwerth, K., and K.M. Belina. 2006. Cover crops enhance soil organic matter, carbon dynamics and microbiological function in a vineyard agroecosystem. *Applied Soil Ecology* 40 (12): 359-369. doi: 10.1016/j.apsoil.2008.06.006.

Stoll, M., and H.G. Jones. 2007. Thermal Imaging as A Viable Tool for Monitoring Plant Stress. *Journal International des Sciences de la Vigne et du Vin* 41(2): 77-84. doi: 10.20870/oeno-one.2007.41.2.851.

Suter, B., R. Triolo, D. Pernet, Z. Dai, C. Van Leeuwen. 2019. Modelling Stem Water Potential by Separating the Effects of Soil Water Availability and Climatic Conditions on Water Status in Grapevine (Vitis vinifera L.). *Frontier in Plant Science*. doi: doi.org/10.3389/fpls.2019.01485

Tanner, C.B. 1963. Plant Temperatures. *Agronomy Journal* 55: 201-211. doi: 10.2134/agronj1963.00021962005500020043x

Turner, N.C. 1990. Plant water relations and irrigation management. *Agricultural Water Management* 17 (1-3): 59-73. doi: 10.1016/0378-3774(90)90056-5

Unmanned-Technologies, 2019, Das System. Retrieved on October 20, 2019 from https://www.unmanned-technologies.de/

Widman, T. 2011. Factors that Influence Cross-validation of Hierarchical Linear Models. Dissertation. Georgia State University.

Williams, L. E., and M.A. Matthews. 1990. Grapevine. *Irrigation of Agricultural Crops*. eds B. A. Stewart and D. R. Nielsen (Madison, WI: ASACSSA-SSSA), 1019–1055.

Williams, L.E., P. Baeza, P. Vaughn. 2012. Midday measurements of leaf water potential and stomatal conductance are highly correlated with daily water use of Thompson Seedless grapevines. *Irrigation Science* 30: 201-212. doi: 10.1007/s00271-011-0276-2

Wu, Y.H., and M.C.Hung. 2016. Comparison of Spatial Interpolation Techniques Using Visualization and Quantitative Assessment. *Intech*. doi: dx.doi.org/10.5772/65996

Yao, X., B. Fu, Y. Lu, F. Sun, S. Wang. 2013. Comparison of Four Spatial Interpolation Methods for Estimating Soil Moisture in a Complex Terrain Catchment. *Plus One* 8(1). doi:10.1371/journal.pone.0054660

Zandi, S., A. Ghobakhlou , P. Sallis. 2011. Evaluation of Spatial Interpolation Techniques for Mapping Soil Ph. 19th International Congress on Modelling and Simulation, Perth, Australia

Zarco-Tejada, P.J., V.Gozales-Dugo, L.E. Williams, L. Suarez, J. Berni, D. Goldhamer, E. Ferers. 2013. A PRI-based water stress index combining structural and chlorophyll effects: Assessment using diurnal narrow-band airborne imagery and the CWSI thermal index. *Remote Sensing of the Environment* 138: 38-50, doi: 10.1016/j.rse.2013.07.024

Appendix 1: cross validation results

Each table provides the following information: the ME and RMSE values for each interpolation method and a rank value which is the product of averaging the rank values given to the ME and RMSE. The lower the value of the ME or the RMSE, the lower the ranking value it received, i.e. 1 is the best possible value.

1.1 Cross-validation results for the Burgweg vineyard for the July 22 session. Number of observations: cover crop: 927,249, grapevine: 150,225.

Burgweg 22_07					
Crop Type	Index	Interpolation	ME	RMSE	Rank Value
Cover	CWSI	Local Polynomial	0.00018	0.027389	1
Cover	CWSI	Kriging	0.000646	0.047471	2
Vine	CWSI	Spline	0.002161	0.054485	3
Vine	CWSI	Kriging	0.001517	0.059745	3
Cover	CWSI	IDW	0.001008	0.070445	3
Cover	Ig	Kriging	0.000829	0.215334	4
Cover	CWSI	Spline	0.005699	0.021666	5
Cover	Ig	Local Polynomial	0.004042	0.201146	5
Cover	Ig	Spline	0.002731	0.266561	5
Vine	CWSI	IDW	0.004516	0.075671	6
Vine	Ig	Kriging	0.003915	0.678277	7
Vine	Ig	Spline	0.00428	0.569879	8
Cover	Ig	IDW	0.012263	0.534819	9
Vine	Ig	IDW	0.020813	1.148779	10
Vine	CWSI	Local Polynomial	0.299205	296.6714	11
Vine	Ig	Local Polynomial	0.397931	882.9908	12

1.2 Cross-validation results for the Burgweg vineyard for the July 25 session. Number of observations: cover crop: 592,589, grapevine: 163,082.

Burgweg 25_07					
Crop Type	Index	Interpolation	ME	RMSE	Rank Value
Cover	CWSI	Spline	9.43E-05	0.016345	1
Cover	CWSI	Local Polynomial	0.000354	0.021064	2
Cover	CWSI	Kriging	0.000151	0.031923	2
Vine	CWSI	Kriging	0.001308	0.04145	3
Vine	CWSI	Spline	0.002374	0.055695	4
Cover	CWSI	IDW	0.001757	0.05972	4
Vine	CWSI	Local Polynomial	0.00425	0.041765	5
Vine	CWSI	IDW	0.004803	0.081106	6
Cover	Ig	Spline	0.003824	0.262723	6
Cover	Ig	Kriging	0.002793	0.279831	7
Cover	Ig	Local Polynomial	0.005246	0.199863	8
Vine	Ig	Spline	0.005303	0.250742	9
Vine	Ig	Kriging	0.004433	0.304133	10
Vine	Ig	Local Polynomial	0.014191	0.268198	11
Vine	Ig	IDW	0.018288	0.449705	12
Cover	Ig	IDW	0.019882	0.520869	13

1.3 Cross-validation results for the Burgweg vineyard for the August 22 session. Number of observations: cover crop: 380,908, grapevine: 489,852.

Burgweg 22_08					
Crop Type	Index	Interpolation	ME	RMSE	Rank Value
Vine	CWSI	Kriging	0.000413	0.024938	1
Cover	CWSI	Local Polynomial	0.00018	0.027389	2
Cover	CWSI	Spline	0.000467	0.030739	3
Vine	CWSI	Local Polynomial	0.002112	0.025504	4
Cover	CWSI	Kriging	0.000646	0.047471	4
Vine	CWSI	Spline	0.001264	0.03564	5
Cover	CWSI	IDW	0.001008	0.070445	6
Vine	CWSI	IDW	0.003185	0.068087	7
Cover	Ig	Local Polynomial	0.004042	0.201146	8
Cover	Ig	Spline	0.00429	0.331041	9
Vine	Ig	Kriging	0.001342	1.807545	10
Cover	Ig	IDW	0.012263	0.534819	11
Vine	Ig	Local Polynomial	0.011645	1.75055	11
Vine	Ig	Spline	0.004322	1.784375	11
Cover	Ig	Kriging	0.096179	0.364923	12
Vine	Ig	IDW	0.020477	1.88187	13

1.4 Cross-validation results for the Burgweg vineyard for the September 19 session. Number of observations: cover crop: 308,508, grapevine: 418,909.

Burgweg 19_09					
Crop Type	Index	Interpolation	ME	RMSE	Rank Value
Cover	CWSI	Spline	3.88E-05	0.014367	1
Cover	CWSI	Local Polynomial	0.000217	0.017071	2
Vine	CWSI	Kriging	0.001485	0.042865	3
Cover	CWSI	IDW	0.001302	0.053916	4
Vine	CWSI	Local Polynomial	0.006163	0.044658	5
Vine	CWSI	Spline	0.003846	0.060245	5
Cover	CWSI	Kriging	1.91E-05	0.657315	5
Vine	Ig	Kriging	0.002349	0.196353	6
Cover	Ig	Spline	0.000862	0.304553	6
Vine	CWSI	IDW	0.009088	0.104389	7
Cover	Ig	Kriging	0.000195	3.317548	7
Cover	Ig	Local Polynomial	0.003969	0.344115	8
Vine	Ig	Local Polynomial	0.018392	0.214813	9
Vine	Ig	Spline	0.012498	0.254125	9
Vine	Ig	IDW	0.034333	0.480662	10
Cover	Ig	IDW	0.02137	0.936896	11

1.5 Cross-validation results for the Ehrenfels vineyard for the July 22 session. Number of observations: cover crop: 1,240,869, grapevine: 90,085.

Ehrenfels 22_07					
Crop Type	Index	Interpolation	ME	RMSE	Rank Value
Cover	CWSI	Kriging	0.000272	0.000272	1
Cover	CWSI	Spline	0.000505	0.026242	2
Vine	CWSI	Spline	0.001165	0.041536	3
Cover	CWSI	Local Polynomial	0.001324	0.026634	4
Vine	CWSI	Kriging	0.000993	0.052746	4
Cover	Ig	Spline	0.001172	0.329049	5
Cover	CWSI	IDW	0.001892	0.062869	6
Vine	CWSI	Local Polynomial	0.00411	0.044447	7
Vine	Ig	Spline	0.002501	0.354833	8
Vine	CWSI	IDW	0.00501	0.079491	9
Cover	Ig	Kriging	0.001658	0.619768	10
Vine	Ig	Kriging	0.004049	0.495264	11
Vine	Ig	Local Polynomial	0.008841	0.371131	12
Cover	Ig	Local Polynomial	0.005162	0.372268	12
Cover	Ig	IDW	0.003872	0.740126	12
Vine	Ig	IDW	0.014109	0.513276	13

1.6 Cross-validation results for the Ehrenfels vineyard for the July 25 session. Number of observations: cover crop: 1,292,708, grapevine: 60,664.

Ehrenfels 25_07					
Crop Type	Index	Interpolation	ME	RMSE	Rank Value
Cover	CWSI	Kriging	0.000133	0.042935	1
Cover	CWSI	Spline	0.001256	0.035127	2
Cover	CWSI	Local Polynomial	0.002961	0.026407	3
Vine	CWSI	Spline	0.001936	0.057345	4
Vine	CWSI	Kriging	0.000707	0.084011	5
Cover	CWSI	IDW	0.002091	0.061303	6
Vine	CWSI	Local Polynomial	0.003906	0.06089	7
Vine	CWSI	IDW	0.00358	0.080157	8
Cover	Ig	Kriging	0.001343	0.382215	8
Vine	Ig	Spline	0.003157	0.269059	9
Cover	Ig	Spline	0.005047	0.247346	10
Cover	Ig	Local Polynomial	0.010309	0.173242	11
Vine	Ig	Kriging	0.004625	0.458307	12
Vine	Ig	IDW	0.009197	0.418595	13
Cover	Ig	IDW	0.006871	0.456929	13
Vine	Ig	Local Polynomial	14.15284	3471.89	14

1.7 Cross-validation results for the Ehrenfels vineyard for the August 22 session. Number of observations: cover crop: 1,007,425, grapevine: 126,112.

Ehrenfels 22_08					
Crop Type	Index	Interpolation	ME	RMSE	Rank Value
Cover	CWSI	Local Polynomial	0.00054	0.028361	1
Cover	CWSI	Spline	0.000656	0.03935	2
Cover	CWSI	IDW	0.000773	0.060166	3
Vine	CWSI	Local Polynomial	0.0055	0.039076	4
Vine	CWSI	Spline	0.002792	0.054577	4
Cover	CWSI	Kriging	0.001942	0.078466	5
Cover	Ig	Spline	0.000349	0.282598	6
Cover	Ig	Local Polynomial	0.000346	0.339707	7
Vine	CWSI	Kriging	0.006315	0.068753	8
Vine	CWSI	IDW	0.006269	0.091244	9
Vine	Ig	Spline	0.007416	0.171699	10
Vine	Ig	Local Polynomial	0.014384	0.138044	11
Cover	Ig	IDW	0.004659	0.717472	11
Vine	Ig	Kriging	0.00843	0.213293	12
Vine	Ig	IDW	0.017656	0.288955	13
Cover	Ig	Kriging	38.1741	210.1981	14

1.8 Cross-validation results for the Ehrenfels vineyard for the September 19 session. Number of observations: cover crop: 889,959, grapevine: 301,521.

Ehrenfels 19_09					
Crop Type	Index	Interpolation	ME	RMSE	Overall Rank
Cover	CWSI	Spline	0.00019	0.014722	1
Cover	CWSI	Local Polynomial	0.00018	0.016408	1
Vine	CWSI	Kriging	0.001175	0.029721	2
Cover	CWSI	IDW	0.000956	0.038542	3
Cover	CWSI	Kriging	0.000157	0.477359	4
Vine	Ig	Kriging	0.000749	0.452145	5
Vine	CWSI	Local Polynomial	0.008556	0.037419	6
Vine	CWSI	Spline	0.004475	0.0572	7
Cover	Ig	Local Polynomial	0.002599	0.222504	7
Vine	Ig	Spline	0.001695	0.422621	8
Cover	Ig	Spline	0.003642	0.345865	9
Cover	Ig	Kriging	0.000892	0.679356	10
Vine	CWSI	IDW	0.014317	0.125863	11
Cover	Ig	IDW	0.008961	0.609818	12
Vine	Ig	Local Polynomial	0.016909	0.490513	13
Vine	Ig	IDW	0.050925	1.096671	14

Appendix 2: Mid-day Ψstem and interpolated surfaces comparison results

2.1 Ψstem to interpolation comparison results for the Burgweg vineyard for the July session.

Burgweg July			
Crop Type	Index	Interpolation	Result
Cover	Ig	Spline	0.967
Cover	CWSI	Spline	0.957
Cover	CWSI	Local Polynomial	0.906
Cover	CWSI	Kriging	0.850
Cover	CWSI	IDW	0.847
Cover	Ig	IDW	0.845
Cover	Ig	Kriging	0.784
Cover	Ig	Local Polynomial	0.778
Vine	Ig	Kriging	0.716
Vine	CWSI	Kriging	0.708
Vine	CWSI	Spline	0.507
Vine	CWSI	Local Polynomial	0.457
Vine	Ig	Local Polynomial	0.327
Vine	CWSI	IDW	0.319
Vine	Ig	IDW	0.175
Vine	Ig	Spline	0.013

2.2 Ψstem to interpolation comparison results for the Burgweg vineyard for the August session.

Burgweg August			
Crop Type	Index	Interpolation	Result
Vine	Ig	Local Polynomial	0.881
Cover	Ig	Local Polynomial	0.854
Cover	CWSI	Local Polynomial	0.854
Vine	Ig	Spline	0.846
Cover	Ig	Spline	0.835
Cover	CWSI	Spline	0.828
Cover	Ig	Kriging	0.812
Cover	CWSI	Kriging	0.811
Cover	Ig	IDW	0.770
Cover	CWSI	IDW	0.733
Vine	Ig	Kriging	0.696
Vine	Ig	IDW	0.695
Vine	CWSI	IDW	0.526
Vine	CWSI	Local Polynomial	0.519
Vine	CWSI	Spline	0.495
Vine	CWSI	Kriging	0.339

2.3 Ψstem to interpolation comparison results for the Burgweg vineyard for the September session.

Burgweg September			
Crop Type	Index	Interpolation	Result
Vine	CWSI	IDW	0.967
Cover	Ig	IDW	0.817
Cover	Ig	Kriging	0.805
Cover	Ig	Local Polynomial	0.801
Cover	Ig	Spline	0.799
Vine	CWSI	Local Polynomial	0.790
Vine	Ig	Local Polynomial	0.787
Vine	CWSI	Kriging	0.775
Cover	CWSI	IDW	0.765
Vine	Ig	IDW	0.757
Vine	Ig	Kriging	0.739
Cover	CWSI	Kriging	0.738
Cover	CWSI	Spline	0.737
Cover	Ig	Local Polynomial	0.666
Vine	Ig	Spline	0.645
Vine	CWSI	Spline	0.645

2.4 Ψstem to interpolation comparison results for the Ehrenfels vineyard for the July session.

Ehrenfels July			
Crop Type	Index	Interpolation	Result
Cover	Ig	IDW	0.679
Cover	Ig	Kriging	0.638
Cover	Ig	Local Polynomial	0.607
Cover	Ig	Spline	0.543
Cover	CWSI	IDW	0.452
Cover	CWSI	Kriging	0.329
Cover	CWSI	Local Polynomial	0.175
Vine	CWSI	Kriging	0.096
Vine	Ig	Kriging	0.074
Vine	Ig	IDW	0.055
Vine	Ig	Local Polynomial	0.003
Cover	CWSI	Spline	0.003
Vine	Ig	Spline	0.002
Vine	CWSI	Local Polynomial	0.001
Vine	CWSI	Spline	0.001
Vine	CWSI	IDW	0.000

2.5 Ψstem to interpolation comparison results for the Ehrenfels vineyard for the August session.

Ehrenfels August			
Crop Type	Index	Interpolation	Result
Vine	Ig	IDW	0.895
Vine	CWSI	IDW	0.887
Cover	CWSI	IDW	0.700
Cover	Ig	IDW	0.573
Cover	CWSI	Kriging	0.523
Cover	Ig	Kriging	0.414
Vine	Ig	Kriging	0.399
Vine	CWSI	Kriging	0.268
Vine	CWSI	Local Polynomial	0.130
Cover	Ig	Local Polynomial	0.108
Vine	Ig	Local Polynomial	0.081
Cover	CWSI	Local Polynomial	0.052
Vine	Ig	Spline	0.036
Vine	CWSI	Spline	0.018
Cover	CWSI	Spline	0.003
Cover	Ig	Spline	0.002

2.6 Ψstem to interpolation comparison results for the Ehrenfels vineyard for the September session.

Ehrenfels September			
Crop Type	Index	Interpolation	Result
Vine	Ig	IDW	0.998
Vine	CWSI	IDW	0.967
Vine	CWSI	Spline	0.890
Vine	CWSI	Local Polynomial	0.762
Cover	Ig	IDW	0.422
Cover	CWSI	IDW	0.366
Cover	CWSI	Local Polynomial	0.342
Vine	Ig	Local Polynomial	0.297
Vine	Ig	Spline	0.230
Vine	Ig	Kriging	0.220
Cover	CWSI	Kriging	0.168
Vine	CWSI	Kriging	0.143
Cover	Ig	Kriging	0.105
Cover	Ig	Spline	0.012
Cover	Ig	Local Polynomial	0.012
Cover	CWSI	Spline	0.010

Appendix 3: Proximal sensitivity and interpolated surfaces comparison results

3.1 Proximal sensitivity to interpolation comparison results for the Burgweg vineyard for the August session.

Burgweg August			
Crop Type	Index	Interpolation	Result
Vine	Ig	Local Polynomial	0.702
Cover	CWSI	Spline	0.680
Cover	Ig	Spline	0.680
Cover	Ig	Local Polynomial	0.656
Cover	CWSI	Local Polynomial	0.634
Cover	CWSI	Kriging	0.609
Cover	Ig	IDW	0.576
Vine	Ig	Kriging	0.556
Cover	CWSI	IDW	0.522
Vine	Ig	IDW	0.482
Vine	CWSI	Local Polynomial	0.473
Vine	CWSI	Spline	0.468
Vine	CWSI	Kriging	0.315
Vine	CWSI	IDW	0.305
Cover	Ig	Kriging	0.252
Vine	Ig	Spline	0.000

3.2 Proximal sensitivity to interpolation comparison results for the Ehrenfels vineyard for the August session.

Ehrenfels August			
Crop Type	Index	Interpolation	Result
Cover	Ig	Local Polynomial	0.997
Cover	CWSI	Local Polynomial	0.961
Vine	Ig	Local Polynomial	0.770
Vine	Ig	Spline	0.712
Cover	Ig	Kriging	0.692
Vine	Ig	Kriging	0.681
Vine	CWSI	Local Polynomial	0.668
Cover	CWSI	Kriging	0.631
Vine	Ig	IDW	0.629
Vine	CWSI	IDW	0.609
Vine	CWSI	Kriging	0.565
Vine	CWSI	Spline	0.436
Cover	Ig	IDW	0.349
Cover	CWSI	Spline	0.257
Cover	CWSI	IDW	0.218
Cover	Ig	Spline	0.054

3.3Proximal sensitivity to interpolation comparison results for the Ehrenfels vineyard for the September session.

Ehrenfels September			
Crop Type	Index	Interpolation	Result
Cover	Ig	Spline	0.999
Cover	CWSI	Spline	0.962
Cover	CWSI	Kriging	0.755
Cover	Ig	Kriging	0.721
Cover	CWSI	IDW	0.598
Cover	CWSI	Local Polynomial	0.584
Cover	Ig	IDW	0.509
Vine	CWSI	Kriging	0.362
Cover	Ig	Local Polynomial	0.339
Vine	CWSI	Local Polynomial	0.282
Vine	Ig	Kriging	0.212
Vine	CWSI	Spline	0.090
Vine	Ig	Local Polynomial	0.045
Vine	Ig	Spline	0.033
Vine	CWSI	IDW	0.017
Vine	Ig	IDW	0.001

Appendix 4: Locations of the ground measurements:

4.1 Locations of the stem water potential:

Date	Vineyard	Lat	Long
22_07	BU	49.975273	7.883259
	BU	49.974998	7.884314
	Ef	49.974908	7.88327
	Ef	49.974837	7.883642
25_07	BU	49.975271	7.883262
	BU	49.974995	7.884306
	Ef	49.974974	7.883086
	Ef	49.974891	7.883452
22_08	BU	49.975235	7.883454
	BU	49.97519	7.883663
	BU	49.975117	7.883926
	BU	49.975019	7.884145
	Ef	49.97497	7.883242
	Ef	49.974938	7.8833
	Ef	49.974921	7.88327
	Ef	49.974863	7.883477
	Ef	49.974863	7.883447
	Ef	49.974835	7.883509
19_09	BU	49.975367	7.883488
	BU	49.975341	7.883338
	Ef	49.97484	7.883466
	Ef	49.974831	7.883172
	Ef	49.974805	7.883725

4.2 Locations of the proximal thermal imaging:

Date	Vineyard	Lat	Long
22/08	BU_1	49.975242	7.883473
	BU-2	49.975237	7.883452
	BU-3	49.975193	7.883662
	BU-4	49.975194	7.883688
	BU-5	49.975134	7.883916
	BU-6	49.975122	7.883924
	BU-7	49.97502	7.884148
	Eh-1	49.974945	7.883244
	Eh-3	49.974936	7.883294
	Eh-2	49.974927	7.883265
	Eh-4	49.974866	7.883444
	Eh-5	49.974866	7.883476
	Eh-6	49.974838	7.883512
19/09	Ef-2	49.974842	7.88347
	Ef-1	49.974832	7.883174
	Ef-3	49.97481	7.883724

Series from Lund University

Department of Physical Geography and Ecosystem Science

Master Thesis in Geographical Information Science

1. *Anthony Lawther:* The application of GIS-based binary logistic regression for slope failure susceptibility mapping in the Western Grampian Mountains, Scotland (2008).
2. *Rickard Hansen:* Daily mobility in Grenoble Metropolitan Region, France. Applied GIS methods in time geographical research (2008).
3. *Emil Bayramov:* Environmental monitoring of bio-restoration activities using GIS and Remote Sensing (2009).
4. *Rafael Villarreal Pacheco:* Applications of Geographic Information Systems as an analytical and visualization tool for mass real estate valuation: a case study of Fontibon District, Bogota, Columbia (2009).
5. *Siri Oestreich Waage:* a case study of route solving for oversized transport: The use of GIS functionalities in transport of transformers, as part of maintaining a reliable power infrastructure (2010).
6. *Edgar Pimiento:* Shallow landslide susceptibility – Modelling and validation (2010).
7. *Martina Schäfer:* Near real-time mapping of floodwater mosquito breeding sites using aerial photographs (2010).
8. *August Pieter van Waarden-Nagel:* Land use evaluation to assess the outcome of the programme of rehabilitation measures for the river Rhine in the Netherlands (2010).
9. *Samira Muhammad:* Development and implementation of air quality data mart for Ontario, Canada: A case study of air quality in Ontario using OLAP tool. (2010).
10. *Fredros Oketch Okumu*: Using remotely sensed data to explore spatial and temporal relationships between photosynthetic productivity of vegetation and malaria transmission intensities in selected parts of Africa (2011).
11. *Svajunas Plunge:* Advanced decision support methods for solving diffuse water pollution problems (2011).
12. *Jonathan Higgins:* Monitoring urban growth in greater Lagos: A case study using GIS to monitor the urban growth of Lagos 1990 - 2008 and produce future growth prospects for the city (2011).
13. *Mårten Karlberg:* Mobile Map Client API: Design and Implementation for Android (2011).
14. *Jeanette McBride:* Mapping Chicago area urban tree canopy using color infrared imagery (2011).
15. *Andrew Farina:* Exploring the relationship between land surface temperature and vegetation abundance for urban heat island mitigation in Seville, Spain (2011).
16. *David Kanyari*: Nairobi City Journey Planner: An online and a Mobile Application (2011).

17. *Laura V. Drews:* Multi-criteria GIS analysis for siting of small wind power plants - A case study from Berlin (2012).
18. *Qaisar Nadeem:* Best living neighborhood in the city - A GIS based multi criteria evaluation of ArRiyadh City (2012).
19. *Ahmed Mohamed El Saeid Mustafa:* Development of a photo voltaic building rooftop integration analysis tool for GIS for Dokki District, Cairo, Egypt (2012).
20. *Daniel Patrick Taylor*: Eastern Oyster Aquaculture: Estuarine Remediation via Site Suitability and Spatially Explicit Carrying Capacity Modeling in Virginia's Chesapeake Bay (2013).
21. *Angeleta Oveta Wilson:* A Participatory GIS approach to *unearthing* Manchester's Cultural Heritage '*gold mine'* (2013).
22. *Ola Svensson:* Visibility and Tholos Tombs in the Messenian Landscape: A Comparative Case Study of the Pylian Hinterlands and the Soulima Valley (2013).
23. *Monika Ogden:* Land use impact on water quality in two river systems in South Africa (2013).
24. *Stefan Rova:* A GIS based approach assessing phosphorus load impact on Lake Flaten in Salem, Sweden (2013).
25. *Yann Buhot:* Analysis of the history of landscape changes over a period of 200 years. How can we predict past landscape pattern scenario and the impact on habitat diversity? (2013).
26. *Christina Fotiou:* Evaluating habitat suitability and spectral heterogeneity models to predict weed species presence (2014).
27. *Inese Linuza:* Accuracy Assessment in Glacier Change Analysis (2014).
28. *Agnieszka Griffin:* Domestic energy consumption and social living standards: a GIS analysis within the Greater London Authority area (2014).
29. *Brynja Guðmundsdóttir:* Detection of potential arable land with remote sensing and GIS - A Case Study for Kjósarhreppur (2014).
30. *Oleksandr Nekrasov:* Processing of MODIS Vegetation Indices for analysis of agricultural droughts in the southern Ukraine between the years 2000-2012 (2014).
31. *Sarah Tressel:* Recommendations for a polar Earth science portal in the context of Arctic Spatial Data Infrastructure (2014).
32. *Caroline Gevaert:* Combining Hyperspectral UAV and Multispectral Formosat-2 Imagery for Precision Agriculture Applications (2014).
33. *Salem Jamal-Uddeen:* Using GeoTools to implement the multi-criteria evaluation analysis - weighted linear combination model (2014).
34. *Samanah Seyedi-Shandiz:* Schematic representation of geographical railway network at the Swedish Transport Administration (2014).
35. *Kazi Masel Ullah:* Urban Land-use planning using Geographical Information System and analytical hierarchy process: case study Dhaka City (2014).
36. *Alexia Chang-Wailing Spitteler:* Development of a web application based on MCDA and GIS for the decision support of river and floodplain rehabilitation projects (2014).
37. *Alessandro De Martino:* Geographic accessibility analysis and evaluation of potential changes to the public transportation system in the City of Milan (2014).

38. *Alireza Mollasalehi:* GIS Based Modelling for Fuel Reduction Using Controlled Burn in Australia. Case Study: Logan City, QLD (2015).
39. *Negin A. Sanati:* Chronic Kidney Disease Mortality in Costa Rica; Geographical Distribution, Spatial Analysis and Non-traditional Risk Factors (2015).
40. *Karen McIntyre:* Benthic mapping of the Bluefields Bay fish sanctuary, Jamaica (2015).
41. *Kees van Duijvendijk:* Feasibility of a low-cost weather sensor network for agricultural purposes: A preliminary assessment (2015).
42. *Sebastian Andersson Hylander:* Evaluation of cultural ecosystem services using GIS (2015).
43. *Deborah Bowyer:* Measuring Urban Growth, Urban Form and Accessibility as Indicators of Urban Sprawl in Hamilton, New Zealand (2015).
44. *Stefan Arvidsson:* Relationship between tree species composition and phenology extracted from satellite data in Swedish forests (2015).
45. *Damián Giménez Cruz*: GIS-based optimal localisation of beekeeping in rural Kenya (2016).
46. *Alejandra Narváez Vallejo:* Can the introduction of the topographic indices in LPJ-GUESS improve the spatial representation of environmental variables? (2016).
47. *Anna Lundgren:* Development of a method for mapping the highest coastline in Sweden using breaklines extracted from high resolution digital elevation models (2016).
48. *Oluwatomi Esther Adejoro:* Does location also matter? A spatial analysis of social achievements of young South Australians (2016).
49. *Hristo Dobrev Tomov:* Automated temporal NDVI analysis over the Middle East for the period 1982 - 2010 (2016).
50. *Vincent Muller:* Impact of Security Context on Mobile Clinic Activities A GIS Multi Criteria Evaluation based on an MSF Humanitarian Mission in Cameroon (2016).
51. *Gezahagn Negash Seboka:* Spatial Assessment of NDVI as an Indicator of Desertification in Ethiopia using Remote Sensing and GIS (2016).
52. *Holly Buhler:* Evaluation of Interfacility Medical Transport Journey Times in Southeastern British Columbia. (2016).
53. *Lars Ole Grottenberg*: Assessing the ability to share spatial data between emergency management organisations in the High North (2016).
54. *Sean Grant:* The Right Tree in the Right Place: Using GIS to Maximize the Net Benefits from Urban Forests (2016).
55. *Irshad Jamal:* Multi-Criteria GIS Analysis for School Site Selection in Gorno-Badakhshan Autonomous Oblast, Tajikistan (2016).
56. *Fulgencio Sanmartín:* Wisdom-volkano: A novel tool based on open GIS and time-series visualization to analyse and share volcanic data (2016).
57. *Nezha Acil:* Remote sensing-based monitoring of snow cover dynamics and its influence on vegetation growth in the Middle Atlas Mountains (2016).
58. *Julia Hjalmarsson:* A Weighty Issue: Estimation of Fire Size with Geographically Weighted Logistic Regression (2016).
59. *Mathewos Tamiru Amato:* Using multi-criteria evaluation and GIS for chronic food and nutrition insecurity indicators analysis in Ethiopia (2016).

60. *Karim Alaa El Din Mohamed Soliman El Attar:* Bicycling Suitability in Downtown, Cairo, Egypt (2016).
61. *Gilbert Akol Echelai:* Asset Management: Integrating GIS as a Decision Support Tool in Meter Management in National Water and Sewerage Corporation (2016).
62. *Terje Slinning:* Analytic comparison of multibeam echo soundings (2016).
63. *Gréta Hlín Sveinsdóttir:* GIS-based MCDA for decision support: A framework for wind farm siting in Iceland (2017).
64. *Jonas Sjögren:* Consequences of a flood in Kristianstad, Sweden: A GIS-based analysis of impacts on important societal functions (2017).
65. *Nadine Raska:* 3D geologic subsurface modelling within the Mackenzie Plain, Northwest Territories, Canada (2017).
66. *Panagiotis Symeonidis*: Study of spatial and temporal variation of atmospheric optical parameters and their relation with PM 2.5 concentration over Europe using GIS technologies (2017).
67. *Michaela Bobeck:* A GIS-based Multi-Criteria Decision Analysis of Wind Farm Site Suitability in New South Wales, Australia, from a Sustainable Development Perspective (2017).
68. *Raghdaa Eissa*: Developing a GIS Model for the Assessment of Outdoor Recreational Facilities in New Cities Case Study: Tenth of Ramadan City, Egypt (2017).
69. *Zahra Khais Shahid*: Biofuel plantations and isoprene emissions in Svea and Götaland (2017).
70. *Mirza Amir Liaquat Baig*: Using geographical information systems in epidemiology: Mapping and analyzing occurrence of diarrhea in urban - residential area of Islamabad, Pakistan (2017).
71. *Joakim Jörwall*: Quantitative model of Present and Future well-being in the EU-28: A spatial Multi-Criteria Evaluation of socioeconomic and climatic comfort factors (2017).
72. *Elin Haettner*: Energy Poverty in the Dublin Region: Modelling Geographies of Risk (2017).
73. *Harry Eriksson*: Geochemistry of stream plants and its statistical relations to soil- and bedrock geology, slope directions and till geochemistry. A GIS-analysis of small catchments in northern Sweden (2017).
74. *Daniel Gardevärn:* PPGIS and Public meetings – An evaluation of public participation methods for urban planning (2017).
75. *Kim Friberg:* Sensitivity Analysis and Calibration of Multi Energy Balance Land Surface Model Parameters (2017).
76. *Viktor Svanerud:* Taking the bus to the park? A study of accessibility to green areas in Gothenburg through different modes of transport (2017).
77. *Lisa-Gaye Greene*: Deadly Designs: The Impact of Road Design on Road Crash Patterns along Jamaica's North Coast Highway (2017).
78. *Katarina Jemec Parker*: Spatial and temporal analysis of fecal indicator bacteria concentrations in beach water in San Diego, California (2017).
79. *Angela Kabiru*: An Exploratory Study of Middle Stone Age and Later Stone Age Site Locations in Kenya's Central Rift Valley Using Landscape Analysis: A GIS Approach (2017).

80. *Kristean Björkmann*: Subjective Well-Being and Environment: A GIS-Based Analysis (2018).
81. *Williams Erhunmonmen Ojo*: Measuring spatial accessibility to healthcare for people living with HIV-AIDS in southern Nigeria (2018).
82. *Daniel Assefa*: Developing Data Extraction and Dynamic Data Visualization (Styling) Modules for Web GIS Risk Assessment System (WGRAS). (2018).
83. *Adela Nistora*: Inundation scenarios in a changing climate: assessing potential impacts of sea-level rise on the coast of South-East England (2018).
84. *Marc Seliger*: Thirsty landscapes - Investigating growing irrigation water consumption and potential conservation measures within Utah's largest master-planned community: Daybreak (2018).
85. *Luka Jovičić*: Spatial Data Harmonisation in Regional Context in Accordance with INSPIRE Implementing Rules (2018).
86. *Christina Kourdounouli*: Analysis of Urban Ecosystem Condition Indicators for the Large Urban Zones and City Cores in EU (2018).
87. *Jeremy Azzopardi*: Effect of distance measures and feature representations on distance-based accessibility measures (2018).
88. *Patrick Kabatha*: An open source web GIS tool for analysis and visualization of elephant GPS telemetry data, alongside environmental and anthropogenic variables (2018).
89. *Richard Alphonce Giliba*: Effects of Climate Change on Potential Geographical Distribution of Prunus africana (African cherry) in the Eastern Arc Mountain Forests of Tanzania (2018).
90. *Eiður Kristinn Eiðsson*: Transformation and linking of authoritative multi-scale geodata for the Semantic Web: A case study of Swedish national building data sets (2018).
91. *Niamh Harty*: HOP!: a PGIS and citizen science approach to monitoring the condition of upland paths (2018).
92. *José Estuardo Jara Alvear*: Solar photovoltaic potential to complement hydropower in Ecuador: A GIS-based framework of analysis (2018).
93. *Brendan O'Neill*: Multicriteria Site Suitability for Algal Biofuel Production Facilities (2018).
94. *Roman Spataru*: Spatial-temporal GIS analysis in public health – a case study of polio disease (2018).
95. *Alicja Miodońska*: Assessing evolution of ice caps in Suðurland, Iceland, in years 1986 - 2014, using multispectral satellite imagery (2019).
96. *Dennis Lindell Schettini*: A Spatial Analysis of Homicide Crime's Distribution and Association with Deprivation in Stockholm Between 2010-2017 (2019).
97. *Damiano Vesentini*: The Po Delta Biosphere Reserve: Management challenges and priorities deriving from anthropogenic pressure and sea level rise (2019).
98. *Emilie Arnesten*: Impacts of future sea level rise and high water on roads, railways and environmental objects: a GIS analysis of the potential effects of increasing sea levels and highest projected high water in Scania, Sweden (2019).
99. *Syed Muhammad Amir Raza*: Comparison of geospatial support in RDF stores: Evaluation for ICOS Carbon Portal metadata (2019).
100. *Hemin Tofiq*: Investigating the accuracy of Digital Elevation Models from UAV images in areas with low contrast: A sandy beach as a case study (2019).

101. *Evangelos Vafeiadis*: Exploring the distribution of accessibility by public transport using spatial analysis. A case study for retail concentrations and public hospitals in Athens (2019).
102. *Milan Sekulic*: Multi-Criteria GIS modelling for optimal alignment of roadway by-passes in the Tlokweng Planning Area, Botswana (2019).
103. *Ingrid Piirisaar*: A multi-criteria GIS analysis for siting of utility-scale photovoltaic solar plants in county Kilkenny, Ireland (2019).
104. *Nigel Fox*: Plant phenology and climate change: possible effect on the onset of various wild plant species' first flowering day in the UK (2019).
105. *Gunnar Hesch*: Linking conflict events and cropland development in Afghanistan, 2001 to 2011, using MODIS land cover data and Uppsala Conflict Data Programme (2019).
106. *Elijah Njoku*: Analysis of spatial-temporal pattern of Land Surface Temperature (LST) due to NDVI and elevation in Ilorin, Nigeria (2019).
107. *Katalin Bunyevácz*: Development of a GIS methodology to evaluate informal urban green areas for inclusion in a community governance program (2019).
108. *Paul dos Santos*: Automating synthetic trip data generation for an agent-based simulation of urban mobility (2019).
109. *Robert O' Dwyer*: Land cover changes in Southern Sweden from the mid-Holocene to present day: Insights for ecosystem service assessments (2019).
110. *Daniel Klingmyr*: Global scale patterns and trends in tropospheric NO2 concentrations (2019).
111. *Marwa Farouk Elkabbany*: Sea Level Rise Vulnerability Assessment for Abu Dhabi, United Arab Emirates (2019).
112. *Jip Jan van Zoonen*: Aspects of Error Quantification and Evaluation in Digital Elevation Models for Glacier Surfaces (2020).
113. *Georgios Efthymiou*: The use of bicycles in a mid-sized city – benefits and obstacles identified using a questionnaire and GIS (2020).
114. *Haruna Olayiwola Jimoh*: Assessment of Urban Sprawl in MOWE/IBAFO Axis of Ogun State using GIS Capabilities (2020).
115. *Nikolaos Barmpas Zachariadis*: Development of an iOS, Augmented Reality for disaster management (2020).
116. *Ida Storm*: ICOS Atmospheric Stations: Spatial Characterization of CO2 Footprint Areas and Evaluating the Uncertainties of Modelled CO2 Concentrations (2020).
117. *Alon Zuta*: Evaluation of water stress mapping methods in vineyards using airborne thermal imaging (2020).